Catena 182 (2019) 104133

Contents lists available at ScienceDirect

Catena

journal homepage: www.elsevier.com/locate/catena

Assessment of chemical weathering and physical erosion along a hillslope, southwest China

Changshun Song[a,c], Hongbing Ji[a,b,*], Howard Omar Beckford[b], Cheng Chang[b], Shijie Wang[a]

[a] State Key Laboratory of Environmental Geochemistry, Institute of Geochemistry, Chinese Academy of Sciences, Guiyang 550002, China
[b] School of Energy and Environmental Engineering, University of Science and Technology Beijing, Beijing 100083, China
[c] Graduate University of the Chinese Academy of Sciences, Beijing 100049, China

ARTICLE INFO

Keywords:
Chemical weathering
Soil erosion
Karst
Soil texture
Element behaviors

ABSTRACT

The chemical compositions and soil erosion characteristics of three soil profiles along a hillslope in karst area, southwest China were investigated. The material sources, element behavior and relationship between soil erosion and soil formation are discussed. Based on the ^{137}Cs technique, the mean soil redistribution rates were found to be 11.88, −15.31 and −21.03 t ha^{-1} year^{-1} in the summit (DSD), shoulder (DSY) and toeslope (DSJ) profiles, respectively. The results show that the three profile soils are in situ weathering products of the underlying bedrocks and have inherited relationships. The Al, rare earth elements (REEs) and high field strength elements (HFSEs) contents increase with increasing clay content in DSY and DSJ profiles, indicating that these elements could be loss with clay particles via soil erosion. Coarse particles contained Si accumulates at the DSJ profile due to the migration of soil from upslope, resulting in Si enrichment. The REEs and HFSEs are mainly transported from the deposition profile DSD as solutes by chemical weathering and from the erosion profiles DSY and DSJ as particles by physical migration. The DSY profile has the thinnest soil layer and lowest clay contents, which facilitate the chemical reaction between minerals and soil water. Above all, we believe that at some intermediate soil erosion rate, that soils with the least input of fresh materials could experience the strongest chemical weathering, resulting in vast dissolution of minerals such as feldspar. These results suggested that soil texture, topographical features and vegetation coverage together affect the soil chemical weathering, physical erosion and element behaviors in karst hillslope.

1. Introduction

Chemical weathering of bedrock occurs within the Critical Zone. This is very important as it affected processes such as the cycling of elements, CO_2 consumption, and soil erosion (Brantley et al., 2007; Braun et al., 2005). Soil is the weathering product of bedrocks and is critical for the sustainable development of ecosystems and human society (Ma et al., 2011a). The study of watershed erosion, as well as element migration, and the biogeochemical cycling of nutrient between the systems of rock, soil and vegetation are usually based on the soil research such as soil provenance and pedogenesis processes (Taylor and Velbel, 1991; Taylor and Lasaga, 1999; Vance et al., 2009). Recently the behaviors of elements during chemical weathering are becoming a research topic of interest, and so various soil profiles on different bedrocks have been studied (Acosta et al., 2011; Babechuk et al., 2014; Gong et al., 2011; Ji et al., 2004; Lucke et al., 2014; Mee et al., 2004; Wei et al., 2013). Chemical weathering produce soils and physical erosion sculpt landscapes, they closely interact to influence the earth surface. Chemical decomposition of bedrock supplies fresh material to physical erosion, while the exposure of fresh material with active surface chemical characteristics is benefit for chemical weathering (Riebe et al., 2004). The weathering profiles formed on hillslopes face severe soil loss due to the topographic gradient driving erosion. Moreover, many human activities, such as cultivation, deforestation, mining and construction of mountain roads, induce soil erosion and then shape soil-mantled hillslopes in combination with chemical weathering.

The karst region (approximately 42.6 × 10^4 km^2) of southwestern China contains approximately 100 million people (Feng et al., 2016). In southwest China, one of the severe environmental problems is soil erosion (Song et al., 2018). Because of anthropogenic activities, the area of this studied hillslope could be exposed to severe soil erosion. The existing soil assessment methods could be grouped as following: the field erosion monitoring (Guo et al., 2015; Jungers et al., 2009); using remote sensing in conjunction with GIS techniques (Fernández and

* Corresponding author at: University of Science and Technology Beijing, Xueyuan Road No. 30, Haidian District, Beijing 100083, China.
E-mail address: ji.hongbing@hotmail.com (H. Ji).

https://doi.org/10.1016/j.catena.2019.104133
Received 16 October 2018; Received in revised form 11 June 2019; Accepted 17 June 2019
Available online 27 June 2019
0341-8162/

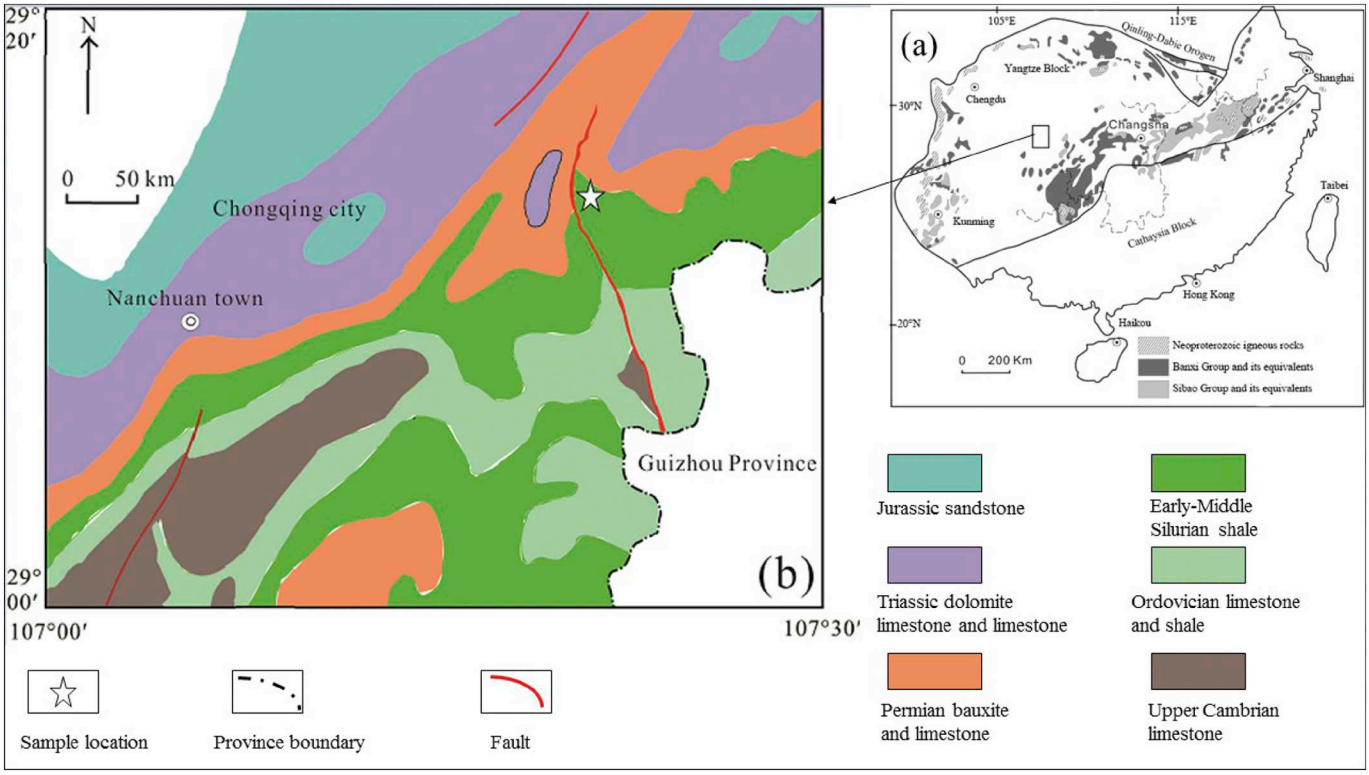

Fig. 1. (a) Sketch map of geology in South China, with the distribution of Meso- to Neoproterozoic strata and magmatism within the Yangtze Block (modified after Gu et al. (2013)); (b) a geologic sketch map illustrating the geological features of the Dafoyan bauxite deposits and sampling site.

Vega, 2016; Yang et al., 2013); and applying the radionuclide techniques of ^{137}Cs, ^{210}Pb and ^{7}Be (Lü et al., 2010; Song et al., 2018; Xiong et al., 2018). Li et al. (2009) proposed that applying the current ^{137}Cs technique to investigate soil erosion on karst regions may be problematic, which is because of the thin layers of soil and dissolution of carbonate particles in soils. However, the much well-developed with thick soil layers, within karst areas of southwest China might be suitable for soil erosion studies using the ^{137}Cs technique. Song et al. (2018) have studied the relationship between major element behaviors and soil erosion on different hillslope components using geochemical methods and the ^{137}Cs technique in southwest China. ^{137}Cs has a half-life of 30.17 years. As an artificial radionuclide produced by nuclear bomb testing, ^{137}Cs was released into the atmosphere first and then deposited on the Earth's surface with precipitation at the period of the 1950s–1970s. Generally, precipitation is usually uniform within small regions, resulting in limited variation of ^{137}Cs inventory in soils. Deposited ^{137}Cs absorbed by fine soil particles (e.g. clay minerals and humic materials) is resistant to chemical or biological removal from soil particles (Rahimi et al., 2013; Zapata, 2002).

Here, we explore the relationship between chemical weathering and physical erosion of hillslope soils with different topographic features located in Chongqing City, southwest China. The specific research objectives of the present study are to (1) investigate the material sources of the hillslope soils; (2) research the formation processes of soil profiles and typical element behaviors during soil formation; and (3) explore the relationship between soil physical erosion and chemical weathering.

2. Materials and methods

2.1. Description of the study area

This study was conducted on a hillslope located in vicinity of the Dafoyan area (29°11′48″–29°15′30″N, 107°20′30″–107°23′00″E) in Nanchuan County, southeastern Chongqing City. The Dafoyan area, which belongs to the Wulong–Nanchuan bauxite deposit cluster, is located in the northwestern South China Block (Fig. 1a). The South China Block includes the Yangtze Block in the northwest and the Cathaysia Block in the southeast. Due to the mild subtropical monsoon climate experienced, temperatures are usually higher during the rainy season. The climate of the study area varies obviously with elevation. The average annual temperature is approximately 17 °C, and the mean annual precipitation is approximately 1400 mm, almost 70% of which occurs from May to August. The mean annual relative humidity is approximately 90%, and the average annual fog period is 260 days.

Representative soil profiles were selected from different components of the hillslope (29°12′45″N, 107°23′46″E), which is located in the Changba syncline (Fig. 1b). The dominant lithology in this hillslope is the dolomite limestone of the Feixianguan and Jialingjiang Formations of the Lower Triassic and the carbonaceous shale of the Hanjiadian Formation of the Early-Middle Silurian. Surveys have revealed that this hillslope was once covered by permanent vegetation, while deforestation occurred at the shoulder and toeslope some 50 years ago due to road construction. Presently there is a mining road at the foot of the studied hillslope. The characteristics of the profiles are summarized in Table 1. The hillslope has an elevation range of 1674 to 1705 m above sea level, and the distance from the toeslope ranges from 0 to 124 m. The slope gradients for the different components, toeslope, shoulder and summit were calculated to be 28.89°, 6.91° and < 5°, respectively. The toeslope profile (DSJ) is located on the side of a mining road with little vegetation coverage, the shoulder profile (DSY) has no vegetation coverage and is located in the center of a relatively flat area with a minor gradient slope, while the summit profile (DSD) is located on the upper slope, on relatively flat area surrounded by scrubland vegetation with a number of trees. Due to the ruggedness of the terrain and elevation, no signs of cultivation on this hillslope.

2.2. Sampling and analytical methods

The soil and bedrock samples were collected in 2014 from three profiles located at the summit (DSD profile), shoulder (DSY profile) and

Table 1
The characteristics of sampling sites in the studied hillslope.

Sample	Land use[a]	Hillslope components	Elevation (m)	Distance[b] (m)	Gradient (°)
DSD	S/F	Summit	1704.08	123.2[c]	< 5
DSY	B	Shoulder	1694.10	40.2	6.91
DSJ	G/B	Toeslope	1674.68	0	28.89

[a] B: bare land; G: grassland; S: scrubland; F: forestland.
[b] The distance from the foot of the hillslope.

toeslope (DSJ profile) of this hillslope. A scraper plate with an internal soil sampling area of 100 cm^2 was used to collect samples at incremental depths (Walling and Quine, 1993), of 2, 5 and 10 cm to a depth of > 25 cm until the bedrock was collected. We also collected two other soil profiles (DFY and ZMXR), which are developed limestones, with depth increments of 20 cm to compare the soil formation processes and element behaviors with those of the hillslope soils. The DFY profile was collected on a flat area near the hillslope, which experienced no obvious soil erosion or deposition. The ZMXR profile, also with no soil erosion or deposition, was sampled farther away from the studied hillslope. Successive rock samples (DFYB) were obtained as chips from a rock profile at approximately 30 cm intervals. Due to the inconsistency of rock outcrops, we collected two types of bedrock in the three soil profiles (DSD, DSY and DSJ): carbonaceous shale (DSD-0) in the DSD profile and dolomite limestone in the DSY and DSJ profiles. Considering the same lithology of bedrocks in DSY and DSJ profiles, we collected one bedrock sample (DSJ-0) for analysis of both soil profiles (DSY and DSJ).

All samples were air-dried and ground to a grain size of 200 mesh. The major element contents of all samples were measured using X-ray fluorescence spectrometry (XRF) (Philips PW2404 X-ray fluorescence spectrometer) and referring to the GB/T14506.28-2010 silicate rock chemical analytical procedure. The trace and rare earth element contents of all samples were analyzed using high-resolution inductively coupled plasma mass spectroscopy (HR-ICP-MS) (Element I, Finnigan MAT Company) according to the DZ/T0223-2001 ICP-MS procedure at a temperature of 20 °C and a humidity of 30%. All these measurements were conducted in the Beijing Research Institute of Uranium Geology.

250 g or more of each soil sample was air-dried and sieved using a 2-mm mesh sieve, then was sent for measurement at the Chengdu Institute of Mountain Hazards and Environment, CAS. A gamma spectrometry system with a hyperpure coaxial germanium detector and a multichannel analyzer was used to measure the ^{137}Cs activity (Bq kg^{-1}). ^{137}Cs activity was detected from the 662 keV peak on the spectrum using counting times > 50,000 s. The analytical precision was kept at approximately ± 5% at the 95% confidence level.

Particle-size distributions of soils were determined followed the hydrometer method (ASTM D422-63), where the proportion of sand, silt and clay in soils were calculated on the basis of hydrometer readings at 40 s and 2 h. Soil pH was determined using a combined glass electrode in deionized water (the ratio of soil (g) to H_2O (mL) was 1:5). We selected surface soil samples (with ^{137}Cs activity) to test particle-size distributions and soil pH. The selected properties of soils are presented in Table 2. The soil in this studied hillslope is classified as mountain yellow soil (Argosols) based on Chinese soil taxonomic classification, which is equivalent to Luvisols in Food and Agriculture Organization (FAO) Taxonomy or Alfisols in United States Department of Agriculture (USDA) Taxonomy (Lin, 2002). The dominant soil texture of the surface soil was determined to be silty loam.

2.3. Elemental mobility

Mass balance calculation, which indicates the loss or enrichment of an element from the soils, is one of the best methods to estimate the element behaviors during various geochemical processes. The tau (τ) mass transport model (Anderson et al., 2002; Brimhall and Dietrich, 1987) was applied for mass balance calculations:

$$\tau_{i,j} = \{[(C_{j,w})/(C_{j,p})]/[(C_{i,w})/(C_{i,p})]\} - 1 \quad (1)$$

where $C_{j,\ w}$ and $C_{j,\ p}$ are the concentrations of element j in soil sample and the parent material, respectively, and $C_{i,\ w}$ and $C_{i,\ p}$ are the contents of the relatively most immobile element (i) in the soil sample and the parent material, respectively. Positive and negative values of $\tau_{i,\ j}$ indicate that the element j was enriched and depleted in the soils respectively, relative to the parent material. A $\tau_{i,\ j}$ value of zero indicates the immobility of the element j in soil samples. Although some studies

Table 2
Surface soil properties in the studied hillslope.

Sample no.	Sand (2–0.02 mm) (%)	Silt (0.02–0.002 mm) (%)	Clay (< 0.002 mm) (%)	pH	Soil texture
DSD-1	32.22417	56.96322	10.81261	5.05	Silty loam
DSD-2	14.20129	73.63703	12.16169	5.12	Silty loam
DSD-3	48.98819	42.88181	8.130006	5.43	Loam
DSD-4	17.24167	69.07538	13.68295	5.28	Silty loam
DSD-5	15.78102	69.60208	14.61689	5.56	Silty loam
DSD-6	43.94643	46.50959	9.543978	5.49	Silty loam
DSD-7	15.03217	72.16187	12.80596	5.32	Silty loam
DSD-8	49.98725	39.63309	10.37967	5.52	Loam
DSD-9	77.54953	18.3623	5.088168	5.79	Sandy loam
DSD10	42.09225	47.80695	10.10081	5.65	Silty loam
DSY-1	12.10816	76.19183	11.70001	6.19	Silty loam
DSY-2	11.67306	75.91682	12.41012	5.97	Silty loam
DSY-3	14.95412	74.79691	10.24897	6.23	Silty loam
DSY-4	11.73725	76.58906	11.67369	5.89	Silty loam
DSY-5	50.1158	43.5401	6.344094	6.36	Loam
DSY-6	44.73591	47.87955	7.384539	6.57	Silty loam
DSY-7	15.96308	72.90047	11.13645	6.79	Silty loam
DSJ-1	25.45452	67.18363	7.361852	5.96	Silty loam
DSJ-2	28.42334	63.98197	7.594695	6.12	Silty loam
DSJ-3	14.60613	73.83325	11.56063	6.34	Silty loam
DSJ-4	14.39751	73.99538	11.60711	6.47	Silty loam
DSJ-5	15.10946	72.28953	12.601	6.35	Silty loam
DSJ-6	15.61089	71.89093	12.49819	6.51	Silty loam
DSJ-7	19.85003	66.98189	13.16808	6.44	Silty loam
DSJ-8	27.41642	59.46671	13.11687	6.67	Silty loam

have used Zr, Th and Nb as the immobile reference element assessing mass balance (Babechuk et al., 2014; Braun et al., 2012; Ma et al., 2007), here, we used Ti as the immobile reference element because Ti is a major element in common rock-forming minerals and is unlikely to suffer from heterogeneity due to its distribution in a trace phase, unlike zircon.

2.4. Estimation of soil erosion and deposition rates

Using the geochemical methods in combination with measurement of the ^{137}Cs activities, we attempted to understand the spatial-temporal distribution of soil erosion and deposition, and the source of sediment. We can estimates of soil redistribution rates of each sampling site by comparison of the ^{137}Cs inventory for an individual sampling site and the ^{137}Cs reference inventory (Quijano et al., 2016).

In this study, assuming that the total fallout of ^{137}Cs occurred in 1963 and that the ^{137}Cs depth distribution in the soil profile is time independent, then the erosion rate Y for an eroding site can be calculated as follows:

$$Y = \frac{10}{t - 1963} \ln\left(1 - \frac{X}{100}\right) h_0 \quad (2)$$

where Y is the annual soil loss (t ha^{-1} a^{-1}) (negative value), t is the year of sampling (year), X is the decreasing relative percentage compared with the local ^{137}Cs reference inventory ($\frac{A_{ref} - A}{A_{ref}} \cdot 100$), A is the total ^{137}Cs inventory at the sampling site by measurement and calculation (Bq m^{-2}). h_0 is an coefficient describing profile shape (kg m^{-2}) driven from an empirical equation ($A'_{(x)} = A_{ref}(1 - e^{-x/h_0})$), where x is the mass depth from soil surface (kg m^{-2}), $A'_{(x)}$ is the concentrations of ^{137}Cs above the depth x (Bq m^{-2}) (Porto et al., 2001; Walling and Quine, 1990; Zhang et al., 1990).

3. Results

3.1. ^{137}Cs records

The vertical distribution of ^{137}Cs activity in the DSD, DSY and DSJ profiles located at the summit, shoulder and toeslope, respectively, of the studied hillslope are illustrated in Fig. 2a, b, and c. Fig. 2a shows that the ^{137}Cs concentration tends to be distributed evenly within the upper 8 cm. At the peak below in activity concentration at depths of 2–4 cm (26.4 Bq kg^{-1}), the profile shows an exponential decrease in ^{137}Cs activity with depth and reaches 0.51 Bq kg^{-1} at a depth of 21 cm. Similar depth distribution profile of ^{137}Cs were observed in Fig. 2b and c. The ^{137}Cs concentration peaks are located at depths of 0–2 cm. Below the peak activity concentration in the topsoil (14.04 Bq kg^{-1}), the ^{137}Cs activity decreases exponentially with increasing depth and reaches 0.53 Bq kg^{-1} at a depth of 14 cm. Fig. 2c shows an distinct exponential decrease in ^{137}Cs activity with depth. Below the ^{137}Cs concentration peak in the surface layer at 2 cm (10.43 Bq kg^{-1}), ^{137}Cs activity decreases exponentially with depth and reaches 0.27 Bq kg^{-1} at a depth of 16 cm.

3.2. Major elements

The major oxide concentrations of samples from the study profiles (DSD, DSY and DSJ) are listed in Table 3. The major element contents of the DFY, DFYB and ZMXR samples are listed in Supplementary Table 1. As shown in Table 3, the oxides SiO_2, Al_2O_3, Fe_2O_3, and MgO and the loss on ignition (LOI) are present in major quantities in all samples from the three sampling sites (accounting for > 97% of the total rock mass), while the other oxides are quite low.

Normally, the accurate isolation and purification of silicate minerals from soils and sediments has proven difficult. Therefore, the correction method proposed by McLennan (1993) is applied in this study. The CIA is calculated based on the average composition of Na and Ca in natural silicate minerals and the molar ratio of CaO/Na_2O in the soil sample, assuming that for CaO* the molar CaO/Na_2O ratio of silicates is not > 1. If this ratio is < 1, the CIA is calculated directly from the molar content of CaO, which is equivalent to m CaO* = m CaO. On the other cases, the CaO content of silicates is supposed to be equivalent to the Na_2O content. The relationship between the chemical index of alteration (CIA) and oxides is shown in Supplementary Fig. 1. The variations in major oxide contents with the CIA indicate the following: (1) The samples from the DSJ profile have higher CIA values, while the CIA values in the samples from the DSD profile are relatively low, (2) compared with the DSD and DSJ profiles, DSY samples are more enriched in less mobile oxides Al_2O_3, TiO_2 and Fe_2O_3 and depleted in the mobile element MgO, (3) the samples from the DSJ profile have widely distributed CIA values, while the samples from the DSY profile are confined within a relatively narrow range of CIA values.

3.3. Trace elements

The trace element concentrations of all samples are listed in Table 4. The Upper Continental Crust (UCC)-normalized abundances of trace elements for the different samples are shown in Supplementary Fig. 2. The UCC-normalized trace element distribution patterns of DSD, DSY and DSJ soil samples are quite similar as a whole. Most samples from the three profiles are enriched in Li, Bi, W, Cd, Sb and Cs and depleted in Cu, Be, Ga, Sc, Rb, Zr, Y, Sr, Ni, Tl, Ba and Hf. However, for individual groups of samples, the concentrations of Cu, Be, Ga, Sc, Rb, Zr and Hf in DSY samples are higher than those in DSD and DSJ samples. Among the three soil profiles, DSY soil samples show higher concentrations of Nb, U, Th, Ta, In, Mo and Zn, and only DSY samples are enriched in these trace elements. DSD soil samples are slightly depleted

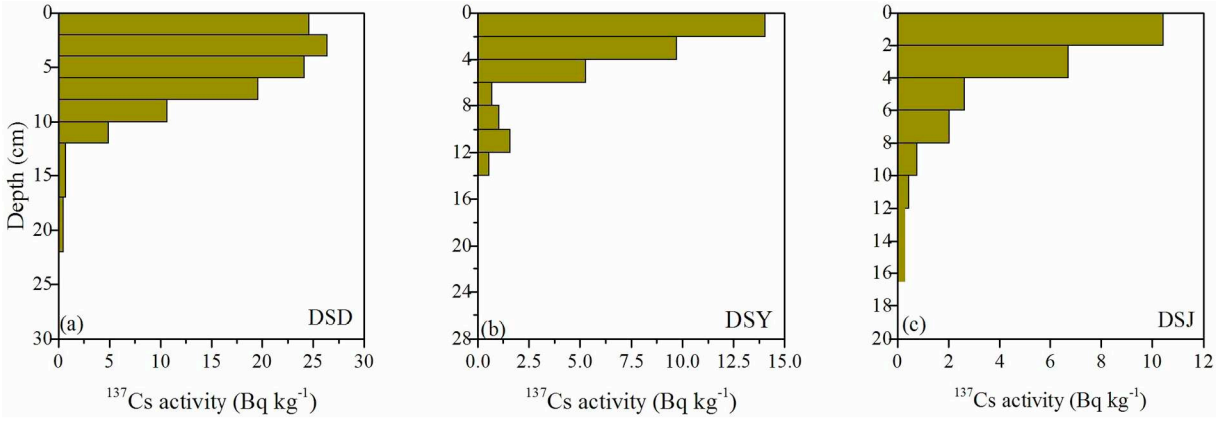

Fig. 2. Depth distribution profiles of ^{137}Cs activity in (a) the summit (DSD), (b) shoulder (DSY) and (c) toeslope (DSJ) component of the hillslope, respectively.

Table 3
The depth distribution of major oxides contents, chemical index of alteration (CIA), and chemical index of weathering (CIW) values of bulk samples from the Dafoyan profiles.

Sample no.	Depth (cm)	Major elements (wt%)											
		SiO_2	Al_2O_3	Fe_2O_3[b]	MgO	CaO	Na_2O	K_2O	MnO	TiO_2	P_2O_5	LOI	CIA[c]	CIW[d]
DSD-0[a]	51	61.39	1.05	0.342	30.66	0.045	0.051	0.071	0.004	0.042	0.012	5.96	81.23	88.46
DSD-1	1 + 2	51.78	6.9	3.01	8.52	0.289	0.233	0.883	0.033	0.469	0.188	27.68	80.02	93.77
DSD-2	3 + 2	53.83	7.1	2.76	8.85	0.243	0.232	0.902	0.029	0.486	0.177	25.08	80.32	94.67
DSD-3	5 + 2	52.21	6.88	2.91	8.69	0.266	0.221	0.858	0.033	0.473	0.166	27.06	80.60	93.86
DSD-4	7 + 2	53.94	6.71	2.84	9.62	0.22	0.224	0.854	0.03	0.46	0.148	24.36	80.15	94.19
DSD-5	9 + 2	58.1	6.74	3.07	10.65	0.223	0.219	0.819	0.03	0.444	0.134	19.3	80.75	93.81
DSD-6	11 + 5	57.46	6.92	3.02	10.66	0.208	0.239	0.836	0.028	0.455	0.13	20.03	80.50	93.77
DSD-7	16 + 5	56.77	7	4.83	9.81	0.201	0.207	0.793	0.033	0.446	0.114	19.41	81.97	94.17
DSD-8	21 + 5	62.03	7.23	3.3	13.4	0.188	0.229	0.792	0.028	0.451	0.087	12.17	82.11	93.41
DSD-9	26 + 5	63.35	6.97	3.25	14.97	0.178	0.2	0.827	0.033	0.458	0.064	9.45	81.83	93.31
DSD10	31 + 10	62.37	5.87	2.59	19	0.156	0.134	0.652	0.026	0.341	0.053	8.51	83.66	93.96
DSD-11	41 + 10	63.89	4.11	1.67	21.29	0.142	0.106	0.364	0.017	0.191	0.036	7.85	84.69	92.23
DSD-12	51	59.88	3.41	1.68	26.44	0.088	0.087	0.279	0.013	0.13	0.034	7.71	85.29	93.90
DSY-1	1 + 2	60.55	9.49	7.34	2.67	0.237	0.237	0.937	0.122	0.54	0.163	17.63	84.10	95.66
DSY-2	3 + 2	58.59	10.96	6.54	2.41	0.241	0.295	1.29	0.153	0.7	0.186	18.51	82.53	95.82
DSY-3	5 + 2	58.23	11.66	6.68	2.75	0.235	0.297	1.34	0.115	0.747	0.182	17.61	83.13	96.05
DSY-4	7 + 2	57.22	11.7	6.32	2.47	0.228	0.311	1.4	0.123	0.76	0.181	19.19	82.74	95.96
DSY-5	9 + 2	60.16	10.76	6.16	2.24	0.227	0.29	1.28	0.122	0.696	0.161	17.88	82.55	95.52
DSY-6	11 + 5	59.38	12.17	5.88	2.61	0.233	0.325	1.45	0.128	0.778	0.175	16.72	82.80	95.76
DSY-7	16 + 5	61.83	12.05	6.91	2.72	0.226	0.295	1.4	0.125	0.771	0.143	13.37	83.32	95.61
DSY-8	21 + 5	70.49	9.25	6.81	2.12	0.228	0.214	1.01	0.127	0.561	0.085	8.78	83.73	94.26
DSY-9	26	65.91	11.15	7.29	2.28	0.211	0.255	1.28	0.13	0.732	0.094	10.32	83.59	95.07
DSJ-0[a]	61	43.99	0.416	0.155	19.63	17.7	0.07	0.04	0.004	0.023	0.009	17.79	60.32	64.37
DSJ-1	1 + 2	66.1	7.48	2.78	5.15	0.25	0.177	0.929	0.07	0.537	0.126	16.17	82.49	94.40
DSJ-2	3 + 2	66.87	8.27	3.73	3.71	0.212	0.185	1.05	0.073	0.617	0.131	14.88	82.57	95.65
DSJ-3	5 + 2	68.12	9.25	3.47	3.04	0.231	0.206	1.16	0.069	0.68	0.132	13.39	82.71	95.43
DSJ-4	7 + 2	69.49	9.07	3.59	3.15	0.204	0.186	1.15	0.061	0.681	0.121	12.03	83.01	95.91
DSJ-5	9 + 2	69.55	9.55	3.83	3.02	0.205	0.193	1.22	0.052	0.728	0.112	11.31	83.00	95.77
DSJ-6	11 + 5	71.59	9.42	3.94	2.76	0.205	0.179	1.2	0.043	0.728	0.093	9.55	83.31	95.49
DSJ-7	16 + 5	73.87	9.04	3.63	2.92	0.263	0.157	1.12	0.025	0.675	0.072	7.82	83.95	94.13
DSJ-8	21 + 5	71.67	8.32	3.26	7.2	0.238	0.137	1.02	0.022	0.615	0.06	7.07	84.26	94.18
DSJ-9	26 + 5	73.31	7.61	4.24	6.35	0.274	0.103	0.749	0.026	0.476	0.05	6.49	86.88	93.28
DSJ-10	31 + 5	63.79	5.26	3.26	18.67	0.221	0.092	0.476	0.017	0.26	0.038	7.58	86.54	91.92
DSJ-11	36 + 5	58.16	7.48	6.07	17.89	0.187	0.1	0.646	0.129	0.321	0.05	8.74	87.91	95.11
DSJ-12	41 + 10	65.07	6.94	4.08	13.93	0.226	0.117	0.692	0.073	0.378	0.06	8.14	85.96	93.79
DSJ-13	51 + 10	63.91	4.35	1.81	21.67	0.198	0.112	0.343	0.024	0.179	0.033	7.03	85.47	90.34
DSJ-14	61	61.88	3.83	1.65	23.88	0.277	0.087	0.285	0.035	0.142	0.031	7.6	86.56	87.00

[a] Stands for bedrock.
[b] Total iron, expressed as Fe_2O_3.
[c] Chemical index of alteration (CIA) = $Al_2O_3 / (Al_2O_3 + CaO^* + Na_2O + K_2O)$, where CaO* only represents the Ca in silicate (calculation reference to McLennan (1993)).
[d] Chemical index of weathering (CIW) = $Al_2O_3 / (Al_2O_3 + CaO^* + Na_2O)$, where CaO* only represents the Ca in silicate (calculation reference to Harnois (1988)

in Cr and V relative to DSY and DSJ samples. Most of the trace elements in all soil samples have experienced no significant fractionation, but Co and Pb experienced relatively obvious fractionation. Compared with soil samples, shale rock samples show a large variation range and have relatively lower contents of the same trace elements but enrichments in Cd and W similar to those in soil samples. The concentrations of Li, Co, Sb and Sr in carbonate rock samples display different enrichment and depletion characteristics.

3.4. Rare earth elements

The REE concentrations and other associated parameters are listed in Table 5. The total REE content (ΣREE) varied within soil profiles which ranges from 50 ppm to 150 ppm with a mean value of approximately 100 ppm. For individual profiles, the mean total REE contents are 70 ppm in DSD samples, 120 ppm in DSY samples, and 92 ppm in DSJ samples. Although the samples have the different REE abundances, the chondrite-normalized REE distributions (Supplementary Fig. 3) of three profile samples are characterized by steep light REE (LREE) patterns. The higher REE concentrations in DSY soil samples are probably present because of the lower concentration of quartz (Hu and Yang, 2016). DSD-11 and DSD-12 have the lowest REE content among DSD soil samples (64.8 ppm and 47.2 ppm, respectively), but they have the highest concentration of SiO_2 (64% and 60%, respectively), consistent with the REE contents of DSY-1 and DSY-8 among DSY soil samples. Among DSJ soil samples, DSJ-12, DSJ-13 and DSJ-14 have the highest REE contents with relatively lower SiO_2 concentrations. The lower contents of REEs in shale rock samples than in soil samples might be associated with the dilution effect of SiO_2 and CaO. Although the shapes of REE patterns are similar, the three soil profiles differ in Ce anomalies. Soil samples from the DSD and DSJ profiles have significant positive Ce anomalies, while samples of the DSY profile do not have distinct Ce anomalies. The bedrock sample from the DSD has positive Ce anomalies, but the bedrock sample from the DSJ profile has negative Ce anomalies.

4. Discussion

4.1. Soil redistribution assessment of the studied hillslope

Zhang et al. (2008) reported a ^{137}Cs reference inventory (1650 Bq m^{-2}) in Kaixian County, Chongqing City. This reference

Table 4
The depth distribution of trace elements contents of bulk samples from Dafoyan profiles.

Samples no.	Depth (cm)	Trace elements (μg/g)													
		Li	Be	Sc	V	Cr	Co	Ni	Cu	Zn	Ga	Rb	Sr	Y	Mo
DSD-0[a]	51	54.1	0.242	1.41	30.8	29.1	4.88	7.36	5.44	13.8	1.57	3.95	3.29	1.75	0.25
DSD-1	1 + 2	39.5	0.605	5.22	75.3	63.1	13	14.2	16.4	70.8	8.31	55.1	40.1	10.1	1.28
DSD-2	3 + 2	42.2	0.751	5.71	74.5	75.5	8.53	14.2	15.5	74	8.68	57.1	40.2	10.8	0.995
DSD-3	5 + 2	42	0.644	5.55	74.2	62.2	22.5	14.7	16	67.3	8.76	48.2	43.3	10.5	1.06
DSD-4	7 + 2	47.9	0.896	5.61	80.6	68.4	17.6	15.7	15.7	70.3	9.39	50.3	37.5	10.7	1.24
DSD-5	9 + 2	43.8	0.817	5.1	76.7	62.3	15.1	13.9	13.7	61.6	8.51	44.9	33.5	9.11	1.15
DSD-6	11 + 5	46.9	0.77	5.93	80	67.5	18.6	15	14.5	60.6	9.25	47.9	39	10.4	1.17
DSD-7	16 + 5	45.3	0.831	5.97	87.8	79.1	46.3	16.7	13.6	59.7	8.84	44	37.3	11	1.26
DSD-8	21 + 5	54.9	0.768	5.96	83.6	74.8	13.9	18.6	12.4	60.3	9.65	45.6	40	10.7	1.01
DSD-9	26 + 5	55.1	1.01	5.98	88.2	72.1	13.4	19.1	12.3	55.9	9.06	45.2	35.7	10.5	0.91
DSD10	31 + 10	61	0.748	5.49	77.5	73.8	15.5	29	12.1	50.5	7.84	37.3	29.2	9.78	0.909
DSD-11	41 + 10	52.8	0.632	4.56	101	89.8	14.3	32.7	14.1	43.2	5.13	26.4	21.7	7.6	0.933
DSD-12	51	56.6	0.517	3.88	52.5	52.3	13.4	25.1	10.9	38	4.51	21.4	12.6	6.22	0.709
DSY-1	1 + 2	34.7	1.59	7.7	118	90.9	39.1	18.3	18.1	91	14.6	66.1	66.2	13.1	2.22
DSY-2	3 + 2	42.7	1.42	9.69	117	93.4	38.6	25.6	23	117	14.4	92	53.6	18.5	2.36
DSY-3	5 + 2	44.3	1.1	10.2	126	110	27.3	27.8	23.1	116	15.7	92.3	54.5	19.6	2.17
DSY-4	7 + 2	46.3	1.26	9.96	120	107	30.3	28	22.3	119	15.1	94.4	56.1	19.9	2.06
DSY-5	9 + 2	43.6	1.21	9.49	114	99.9	35	27.3	22.5	113	15.1	93.7	55.4	18.9	2.07
DSY-6	11 + 5	48.4	1.21	10.2	115	100	30.5	29.5	23.8	119	15.7	98.7	58	18.9	1.86
DSY-7	16 + 5	44.6	1.5	10.5	126	113	27.2	30.2	22.6	116	15.7	97.8	61	17.6	2.24
DSY-8	21 + 5	32.9	1.46	7.96	102	106	40.4	23.1	17.6	78.7	12.3	69	48.6	13.5	2.44
DSY-9	26	40.5	1.84	10.8	120	106	41.9	29.4	22.5	85.1	15.6	89.3	55.7	19.2	2.4
DSJ-0[a]	61	30.6	0.141	0.554	25.5	29.3	2.74	13.3	2.59	11.1	0.646	1.87	549	4.17	0.556
DSJ-1	1 + 2	34.5	0.949	7.02	78.6	81.4	91.6	17.5	16.7	74.5	8.13	58.8	41.2	13.9	1.15
DSJ-2	3 + 2	33.4	0.934	6.53	67.6	92.8	35.3	18.9	17.2	65.8	9.41	58.4	38.6	13.4	1.05
DSJ-3	5 + 2	36.4	1.05	7.28	84.4	85	31	19.8	18.9	65.3	9.92	64.4	42.6	14.3	5.08
DSJ-4	7 + 2	39.2	1.29	7.42	76.7	89.3	37.6	20.8	18.6	68.2	10.3	66.9	42.5	13.4	1.3
DSJ-5	9 + 2	38.2	0.97	7.65	71.6	87.3	37.8	19.8	18.9	67	10.1	65.5	42	12.2	1.44
DSJ-6	11 + 5	38.9	1.32	7.3	72.6	87.2	29.4	20.4	18.5	65.2	10.1	65.6	42.1	11.5	1.02
DSJ-7	16 + 5	39.9	1.02	7.97	84.1	78.2	35.4	22.3	19	66.8	10.6	68.2	45.1	12.8	1.57
DSJ-8	21 + 5	43	1.15	8.27	104	103	24.1	24.9	19.2	64.3	11	66.9	53.5	13.5	1.18
DSJ-9	26 + 5	42.7	1.53	7.71	112	157	51.1	32.1	17.3	63.7	10	43.8	47.9	10.7	1.92
DSJ-10	31 + 5	51.4	1.19	6.09	90.1	95.6	16.6	24.9	20.4	49.4	6.03	28.5	30.9	7.84	3.79
DSJ-11	36 + 5	62.8	2.52	10.2	98.6	140	20.9	34.9	20.3	64.4	8.77	39.2	26.6	14.8	3.07
DSJ-12	41 + 10	52.7	2.35	8.65	95.1	105	19.4	29.5	16.8	59.2	7.58	39	32.5	18.1	1.78
DSJ-13	51 + 10	54.5	1.6	5.31	70	79.8	12.6	25.5	12.3	40.7	4.6	21.9	19.4	18.4	0.8
DSJ-14	61	56.4	3.03	5.06	52.3	72.6	7.58	28.4	10.6	36	4.1	18.6	19.9	47.6	0.833

Samples no.	Trace elements (μg/g)															
	Cd	In	Sb	Cs	Ba	W	Re	Tl	Pb	Bi	Th	U	Nb	Ta	Zr	Hf
DSD-0[a]	0.119	0.006	0.171	0.828	16	4.17	< 0.002	0.069	4.32	0.038	0.802	0.98	0.778	0.064	7.11	0.19
DSD-1	0.721	0.045	1.69	6.42	169	39.7	< 0.002	0.408	42.5	0.605	6.24	2.11	9.66	0.743	65.5	1.82
DSD-2	0.692	0.047	1.37	5.8	176	32.8	0.002	0.402	71.3	0.41	6.25	2.18	9.08	0.631	68.6	1.97
DSD-3	0.65	0.041	1.32	5.72	156	79.2	0.003	0.393	29.9	0.404	5.51	1.77	9.05	0.641	67.4	1.86
DSD-4	0.568	0.039	1.11	5.88	164	65.4	< 0.002	0.415	27.6	0.363	5.57	1.91	9.48	0.638	65.5	1.81
DSD-5	0.39	0.032	0.969	5.36	147	83.4	0.005	0.353	24.4	0.288	5.07	1.72	8.59	0.545	57.9	1.62
DSD-6	0.373	0.036	0.907	5.75	159	46	0.002	0.374	26	0.307	5.31	1.83	9.12	0.632	64.4	1.84
DSD-7	0.484	0.036	0.909	5.5	154	240	0.009	0.399	24.2	0.283	5.72	1.95	8.91	0.61	65	1.74
DSD-8	0.275	0.051	0.785	5.76	155	35.2	< 0.002	0.364	19.9	0.298	6.67	2.01	9.48	0.638	64.9	1.89

(*continued on next page*)

Table 4 (*continued*)

Samples no.	Trace elements (μg/g)															
	Cd	In	Sb	Cs	Ba	W	Re	Tl	Pb	Bi	Th	U	Nb	Ta	Zr	Hf
DSD-9	0.212	0.043	0.738	5.61	150	33.6	0.002	0.372	18.9	0.293	7.24	1.97	9.32	0.64	67.7	1.93
DSD10	0.24	0.034	0.682	4.63	115	22	< 0.002	0.291	15.8	0.277	6.45	1.93	7	0.463	58	1.57
DSD-11	0.302	0.027	0.758	3.51	79.5	19.3	0.003	0.271	15.6	0.281	5.55	2.56	4.52	0.322	38.5	1.18
DSD-12	0.271	0.026	0.517	2.85	61.8	20	0.002	0.233	11.4	0.19	3.64	1.89	3.07	0.231	26.7	0.839
DSY-1	0.523	0.07	1.68	6.58	215	153	0.006	0.427	38.1	0.45	9.75	2.98	12.3	0.898	94.5	2.81
DSY-2	0.619	0.063	1.75	9.11	302	79.9	0.003	0.637	47.6	0.527	11.5	3.24	16.6	1.19	129	3.91
DSY-3	0.461	0.065	1.72	9.36	316	60.1	0.003	0.598	43.2	0.508	12.1	3.43	17.2	1.26	135	4.07
DSY-4	0.431	0.051	1.44	10.3	330	59.9	0.004	0.669	43.5	0.512	12.3	3.47	18	1.31	138	4.1
DSY-5	0.332	0.071	1.58	9.66	312	88.1	0.005	0.594	41.6	0.508	11.9	3.45	17.1	1.26	125	3.76
DSY-6	0.433	0.068	1.51	10.5	342	77.5	0.004	0.665	41.4	0.503	12.5	3.42	18.5	1.44	123	3.74
DSY-7	0.386	0.061	1.45	10.3	336	54.8	0.005	0.636	37.7	0.513	13.7	3.56	18.4	1.39	116	3.65
DSY-8	0.284	0.056	1.51	7.13	249	134	0.005	0.487	32.5	0.382	10.9	2.98	13	1.02	93.6	3.02
DSY-9	0.278	0.057	1.8	8.98	299	118	0.002	0.555	36.7	0.466	13.7	4.12	17.1	1.34	134	4.34
DSJ-0[a]	1.31	0.003	0.195	0.391	6.85	16.3	0.012	0.079	1.12	0.032	0.303	1.72	0.441	0.038	3.63	0.095
DSJ-1	0.669	0.045	1.22	5.94	211	454.2	0.01	0.394	30.7	0.351	6.63	2.18	10.2	0.921	77.2	2.23
DSJ-2	0.565	0.043	1.17	6.51	204	141	0.004	0.406	28.8	0.34	7.18	2.26	11.9	0.86	89.1	2.65
DSJ-3	0.342	0.044	1.11	7.14	226	113	0.003	0.442	30.2	0.374	8.47	2.32	13.3	0.912	97.2	2.83
DSJ-4	0.298	0.049	1.09	7.46	227	142	0.004	0.437	27.5	0.359	8.64	2.4	13.3	0.921	96.2	2.77
DSJ-5	0.261	0.047	1.14	7.3	229	143	0.005	0.429	27	0.342	8.5	2.27	13.5	0.966	87.2	2.57
DSJ-6	0.322	0.041	1.14	7.32	231	110	0.004	0.437	24.5	0.339	8.57	2.34	14.1	1.02	83.5	2.39
DSJ-7	0.277	0.043	1.21	7.71	234	138	0.003	0.421	23	0.341	9.28	2.53	14.5	1.03	95.9	2.71
DSJ-8	0.326	0.047	1.33	7.8	241	90.3	0.003	0.453	20.4	0.339	9.66	2.83	14.4	1.04	104	3.09
DSJ-9	0.523	0.052	1.41	5.37	185	228	0.006	0.353	17.9	0.33	8.83	4.19	9.71	0.683	77.2	2.23
DSJ-10	0.486	0.028	1.35	3.95	112	47.7	< 0.002	0.25	13.6	0.22	5.26	2.88	5.23	0.353	41.3	1.28
DSJ-11	1.52	0.042	1.44	5.43	131	7.19	< 0.002	0.525	19.4	0.301	7.05	4	6.37	0.458	55.6	1.6
DSJ-12	1.02	0.037	0.908	5.05	133	33.3	0.003	0.386	15.9	0.257	6.32	3.4	7.47	0.528	60.2	1.73
DSJ-13	0.784	0.025	0.608	3	76.4	19.1	0.002	0.248	9.77	0.159	3.71	2.51	3.87	0.26	31.1	0.845
DSJ-14	3.47	0.022	0.686	2.72	68.8	13.6	0.003	0.305	8.17	0.147	2.81	2.76	2.78	0.197	26.3	0.767

[a] Bedrock.

Table 5
Rare earth elements contents and relative parameters of bulk samples from Dafoyan profiles.

Samples no.	Depth (cm)	Rare earth elements (μg/g)																						
		La	Ce	Pr	Nd	Sm	Eu	Gd	Tb	Dy	Ho	Er	Tm	Yb	Lu	LREE	HREE	L/H[b]	ΣREE[b]	δCe[b]	δEu[b]	La_N/Sm_N[b]	Gd_N/Yb_N[b]	La_N/Yb_N[b]
DSD-0[a]	51	1.41	5.14	0.31	1.09	0.23	0.063	0.233	0.046	0.277	0.053	0.154	0.023	0.15	0.02	8.24	0.96	8.62	9.20	1.87	0.83	3.85	1.26	6.33
DSD-1	1 + 2	15.8	35.7	3.46	12.3	2.31	0.386	1.87	0.293	1.7	0.35	1	0.166	0.998	0.155	69.96	6.53	10.71	76.49	1.16	0.57	4.30	1.52	10.66
DSD-2	3 + 2	15.7	36	3.33	12.4	2.43	0.393	2.08	0.322	2.02	0.356	1.02	0.177	1.11	0.161	70.25	7.25	9.70	77.50	1.20	0.53	4.06	1.52	9.53
DSD-3	5 + 2	15.4	35.4	3.26	12	2.15	0.396	1.87	0.313	1.77	0.346	1.01	0.174	1.07	0.156	68.61	6.71	10.23	75.32	1.20	0.60	4.50	1.41	9.69
DSD-4	7 + 2	15.8	36.8	3.32	12.5	2.18	0.389	1.96	0.305	1.71	0.334	1.04	0.175	1.02	0.152	70.99	6.70	10.60	77.69	1.22	0.58	4.56	1.55	10.43
DSD-5	9 + 2	14	32.6	3.03	10.9	1.83	0.375	1.7	0.292	1.5	0.322	0.905	0.157	0.948	0.138	62.74	5.96	10.52	68.70	1.21	0.65	4.81	1.45	9.95
DSD-6	11 + 5	14.7	34.9	3.16	12.2	1.98	0.366	1.69	0.3	1.71	0.345	1.05	0.159	1.05	0.146	67.31	6.45	10.44	73.76	1.23	0.61	4.67	1.30	9.43
DSD-7	16 + 5	15	36	3.36	12.1	2.16	0.414	1.77	0.341	1.82	0.352	1.05	0.177	1.14	0.153	69.03	6.80	10.15	75.84	1.22	0.65	4.37	1.26	8.86
DSD-8	21 + 5	15.3	46.8	3.34	12.5	2.23	0.441	1.94	0.333	1.88	0.35	1.05	0.175	1.07	0.149	80.61	6.95	11.60	87.56	1.58	0.65	4.31	1.47	9.63
DSD-9	26 + 5	14.7	53.4	3.08	11.5	2.12	0.441	2.02	0.333	1.85	0.349	0.971	0.183	1.02	0.157	85.24	6.88	12.38	92.12	1.91	0.65	4.36	1.60	9.71
DSD10	31 + 10	11.4	54.6	2.6	9.46	1.82	0.333	1.59	0.307	1.72	0.337	0.96	0.161	1.01	0.126	80.21	6.21	12.91	86.42	2.42	0.60	3.94	1.27	7.60
DSD-11	41 + 10	8.76	39.2	1.92	7.42	1.66	0.326	1.54	0.268	1.51	0.266	0.791	0.129	0.855	0.116	59.29	5.48	10.83	64.76	2.30	0.62	3.32	1.46	6.90
DSD-12	51	6.24	28.4	1.38	5.54	1.25	0.237	1.08	0.218	1.18	0.22	0.62	0.105	0.603	0.085	43.05	4.11	10.47	47.16	2.33	0.62	3.14	1.45	6.97
DSY-1	1 + 2	19.7	42.2	4.26	16.2	2.85	0.53	2.54	0.438	2.22	0.485	1.46	0.224	1.54	0.222	85.74	9.13	9.39	94.87	1.11	0.60	4.34	1.33	8.62
DSY-2	3 + 2	27.7	59.1	5.78	21.2	3.9	0.785	3.38	0.616	3.21	0.648	2.06	0.317	2.11	0.29	118.47	12.63	9.38	131.10	1.13	0.66	4.46	1.30	8.84
DSY-3	5 + 2	28.8	63	6.11	22.7	4	0.756	3.7	0.668	3.35	0.673	2.14	0.329	2.22	0.318	125.37	13.40	9.36	138.76	1.14	0.60	4.53	1.35	8.74
DSY-4	7 + 2	28.9	63.7	6.2	23.9	4.25	0.811	3.67	0.683	3.49	0.683	2.12	0.355	2.26	0.338	127.76	13.60	9.39	141.36	1.15	0.63	4.27	1.31	8.61
DSY-5	9 + 2	28.5	63.6	6.21	22.9	4.17	0.825	3.57	0.644	3.3	0.656	2.09	0.336	2.25	0.309	126.21	13.16	9.59	139.36	1.15	0.65	4.30	1.28	8.53
DSY-6	11 + 5	30.2	66.5	6.46	24.3	4.31	0.833	3.75	0.634	3.22	0.647	2.14	0.329	2.16	0.313	132.60	13.19	10.05	145.80	1.15	0.63	4.40	1.40	9.42
DSY-7	16 + 5	31.5	67.7	6.75	25.9	4.52	0.805	3.88	0.651	3.17	0.661	1.9	0.333	2.13	0.306	137.18	13.03	10.53	150.21	1.12	0.59	4.38	1.47	9.96
DSY-8	21 + 5	15.3	46.8	3.34	12.5	2.23	0.441	1.94	0.333	1.88	0.35	1.05	0.175	1.07	0.236	102.48	9.81	10.45	112.29	1.29	0.60	4.32	1.26	8.56
DSY-9	26	14.7	53.4	3.08	11.5	2.12	0.441	2.02	0.333	1.85	0.349	0.971	0.183	1.02	0.338	128.58	13.50	9.52	142.08	1.27	0.63	4.30	1.21	7.76
DSJ-0[a]	61	5.49	1.46	0.854	3.01	0.45	0.098	0.411	0.064	0.37	0.085	0.244	0.031	0.213	0.031	11.36	1.45	7.84	12.81	0.16	0.70	7.67	1.56	17.36
DSJ-1	1 + 2	17.2	44.2	3.86	14.4	2.67	0.48	2.35	0.412	2.31	0.471	1.37	0.236	1.47	0.202	82.81	8.82	9.39	91.63	1.31	0.59	4.05	1.29	7.88
DSJ-2	3 + 2	18.1	43.5	3.88	14.8	2.49	0.488	2.21	0.404	2.16	0.448	1.37	0.232	1.47	0.206	83.26	8.50	9.80	91.76	1.25	0.64	4.57	1.22	8.29
DSJ-3	5 + 2	19.6	50.2	4.19	15.8	2.66	0.459	2.37	0.42	2.26	0.471	1.45	0.25	1.63	0.209	92.91	9.06	10.25	101.97	1.33	0.56	4.63	1.18	8.10
DSJ-4	7 + 2	20.1	51.6	4.24	16.1	2.6	0.462	2.52	0.407	2.29	0.464	1.43	0.247	1.47	0.219	95.10	9.05	10.51	104.15	1.35	0.55	4.86	1.39	9.21
DSJ-5	9 + 2	19.5	50.1	4.19	15.4	2.55	0.468	2.23	0.388	2.07	0.417	1.28	0.223	1.39	0.199	92.21	8.20	11.25	100.41	1.34	0.60	4.81	1.30	9.45
DSJ-6	11 + 5	19.7	48.6	4.27	15.4	2.54	0.442	2.26	0.373	1.9	0.353	1.14	0.2	1.29	0.178	90.95	7.69	11.82	98.65	1.28	0.56	4.88	1.42	10.28
DSJ-7	16 + 5	20	47.4	4.3	15.9	2.71	0.483	2.43	0.394	2.03	0.431	1.31	0.214	1.4	0.215	90.79	8.42	10.78	99.22	1.23	0.58	4.64	1.40	9.62
DSJ-8	21 + 5	19.4	50.9	4.16	15.3	2.62	0.452	2.25	0.398	2.18	0.463	1.45	0.25	1.45	0.209	92.83	8.65	10.73	101.48	1.36	0.57	4.65	1.26	9.01
DSJ-9	26 + 5	13.4	60	2.88	10.6	1.87	0.346	1.8	0.299	1.81	0.361	1.08	0.199	1.26	0.182	89.10	6.99	12.74	96.09	2.33	0.58	4.50	1.16	7.16
DSJ-10	31 + 5	8.25	42.2	1.85	6.82	1.33	0.247	1.32	0.244	1.37	0.25	0.791	0.131	0.809	0.115	60.70	5.03	12.07	65.73	2.60	0.57	3.90	1.32	6.87
DSJ-11	36 + 5	13.2	64.3	3.21	12.1	2.54	0.533	2.46	0.493	2.63	0.499	1.51	0.232	1.62	0.213	95.88	9.66	9.93	105.54	2.38	0.65	3.27	1.23	5.49
DSJ-12	41 + 10	16.1	53.3	4.2	15.8	3.53	0.697	2.89	0.6	3.18	0.623	1.77	0.308	1.88	0.253	93.63	11.50	8.14	105.13	1.56	0.67	2.87	1.24	5.77
DSJ-13	51 + 10	15.6	31.4	3.65	13.7	3.04	0.663	2.66	0.52	2.8	0.548	1.57	0.251	1.37	0.203	68.05	9.92	6.86	77.98	1.00	0.71	3.23	1.57	7.67
DSJ-14	61	43.4	23.1	8.49	33.2	5.99	1.26	5.47	0.956	4.81	1.01	2.79	0.41	2.43	0.349	115.44	18.23	6.33	133.67	0.29	0.67	4.55	1.82	12.03

[a] Bedrock.
[b] L/H represents the concentration ratio of LREE and HREE. ΣREE = the sum of all rare earth elements, $\delta Ce = Ce_N / (La_N \times Pr_N)^{0.5}$, $\delta Eu = Eu_N / (Sm_N \times Gd_N)^{0.5}$, La_N / Sm_N, Gd_N / Yb_N and La_N / Yb_N, where N refers to a chondrite-normalized value.

Table 6
The ^{137}Cs inventories and soil redistribution at different hillslope components.

Sample	Hillslope components	^{137}Cs inventory (Bq m^{-2})	Soil redistribution (t ha^{-1} year^{-1})
DSD	Summit	2698.56	11.88
DSY	Shoulder	875.55	−15.31
DSJ	Toeslope	690.82	−21.03

profile was collected in 2004 and is located in flat grassland. The county has a subtropical climate similar to that of Nanchuan County, with an average annual rainfall of 1100 mm. Considering the short distance between the reference site and this study area and the similar climate conditions, we use this reference inventory to calculate the soil redistribution rates. The ^{137}Cs inventories and soil redistribution rates of three soil profiles are shown in Table 6. The ^{137}Cs inventories are 2698.56, 875.55, and 690.82 Bq m^{-2} at the DSD profile, DSY profile and DSJ profile, respectively. The ^{137}Cs inventories of the DSY and DSJ soil profiles are lower than the ^{137}Cs reference inventory (1650 Bq m^{-2}). This result indicates that soil erosion occurred at the DSY profile and DSJ profile, whereas soil deposition occurred only at the DSD profile. From Eq. 2, the annual redistribution rates were calculated to be 11.88, −15.31 and −21.03 t ha^{-1} year^{-1} at the summit, shoulder and toeslope of the studied hillslope, respectively. These results are different from other scholars, who proposed that the highest degree of soil erosion occurred at the shoulder and the lowest at the toeslope (Ayoubi et al., 2012; Rahimi et al., 2013). While those phenomena often occurred in single-factor cases, which are different from this studied hillslope due to various of topographical features, land use types in each hillslope component (Song et al., 2018).

Song et al. (2018) have reported that soil deposition occurred at the shoulder of a karst hillslope in Guangxi province, due to good vegetation coverage. Similarly, summit component, with relatively flat terrain and good vegetation coverage lead to the lower velocity and flux of surface runoff, which reduce soil erosion in hillslope. Although this component is relative flat, it is located at the middle of an unapparent depression. We suggest that the sediment transported from the surrounding area via runoff and animal activities lead to the deposition. The soil erosion in the shoulder component could be attribution to surface soil erosion due to no vegetation coverage that can protect the soil against erosion. On the toeslope component, the low vegetation coverage coupled with the high slope gradient could contribute to the greatest erosion rate. Especially a mountain road exists at the foot of the hillslope, resulting in frequent human activities near the toeslope component. It is thus reasonable to assume that eroded material from higher components is easier to be carried away from soil surface by runoff, especially fine particles. The open environment of the toeslope component due to the construction of road is more suitable for soil solution and soil particles migration from the lower section of toeslope profile. These results indicate that the ^{137}Cs activity and inventory, as well as erosion/deposition, were significantly affected by terrain factors (i.e., slope gradient, land use type and amount of vegetation cover) and the interference of human activities (i.e., deforestation and the construction of roads). The organic matter and fine soil particles contribute to the calculation of deposition rate in summit component, because ^{137}Cs is easily and strongly absorbed by humic materials and clay minerals (Zapata, 2002). While, the good vegetation coverage enhanced the clay formation via chemical weathering and organic matter decomposition, we also suggest that the increasing efforts of vegetation protection, rehabilitation, reforestation and reducing interference of human activities are the important approaches to reduce soil erosion in karst hillslopes in this area.

4.2. Effects of clay content and profile characteristics on soil elements

Soil texture (usually soil clay content) has been used to study the physical, chemical and biological processes that occur in soils and ecosystems (Bruun et al., 2010). Ge et al. (2019) examined the influences of soil texture on the distribution of Organic Carbon and nutrients of aggregates over various land use. In this section, we investigate the effect of soil texture (clay content) on soil element behaviors in erosion profiles (DSY and DSJ) and deposition profile (DSD). As shown in Fig. 3, we observed significant increases in the contents of Al_2O_3, HFSEs and REEs in the erosion profile (DSY and DSJ) and decreases in the SiO_2 contents in the DSD and DSY profiles with clay content. The clay materials is easily loss from soil surface during erosion process due to runoff and topographical features (Quijano et al., 2016; Walling and Quine, 1990; Zapata, 2002). Considering the soil erosion characteristics in these three soil profiles (as discussed in Section 4.1), soil deposition occurred at summit component (DSD) of this hillslope and erosion occurred at the shoulder (DSY) and toeslope (DSJ). In the erosion profiles (DSY and DSJ), the increase in Al content with increasing clay content was primarily due to the physical migration of an Al-rich phase (e.g., clay minerals) with soil erosion (Maynard, 1992; Young and Nesbitt, 1998). Clay mineral adsorption plays an important role in distribution of trace element including HFSEs (Liu, 2009). REEs usually adsorbed onto clay minerals after released in solution and are then transported along with clay minerals (Ma et al., 2011b; Su et al., 2017). The relationships of HFSEs and REEs in the DSY and DSJ profiles might be due to the physical migration of HFSEs and REEs with clay minerals during soil erosion process. As discussed above, clay minerals significantly affected the redistributions and behaviors of Al, HFSEs and REEs due to the Adhesive properties (binding sites) and chemical charge cation Al^{3+} (Ge et al., 2019). However, the concentrations of Al, HFSEs and REEs in the deposition profile (DSD), were relatively low in clay content indicating that chemical migration might be responsible the transportation of minerals via soil solution. The low pH values and well vegetation coverage of the DSD profile enhance the migration of Al, HFSEs and REEs as solutes in soil water (Braun et al., 2017; Jin et al., 2010). The Si contents, however decreases with increasing of clay content in the DSD and DSY profiles, suggesting that clay may not be the main carrier. The loss of Si might be due to the dissolution of feldspar by soluble loads. These results further highlighted the importance of soil texture and profile characteristics in the redistributions and behaviors of soil elements especially trace elements. The behaviors of soil elements in each hillslope component during chemical weathering and soil erosion were discussed below (in Sections 4.4 and 4.5).

4.3. The material sources of the soils

Among the major elements, Ti, Al and Fe are considered to be less mobile (Ji et al., 2004) and possesses the lowest solubility in natural water (except in the Fe(II) form) (Hu and Yang, 2016). The TiO_2/Al_2O_3 ratio is generally used to determine the material sources of sediments and sedimentary rocks (Young and Nesbitt, 1998), and Fe_2O_3/Al_2O_3 is also an effective indictor in tracing material sources (Ji et al., 2004). The relationships between Al_2O_3 and TiO_2 (Fig. 4a) show that soil samples from the DSD, DSY and DSJ profiles have significant positive correlations ($R^2 = 0.93$) with their underlying substrates, but the contents of Al_2O_3 in DFY samples have no significant correlation with the increasing TiO_2 contents (distributed as a horizontal line). The successive rock samples have higher TiO_2 and Al_2O_3 concentrations with no visible correlation between the two major oxides. The relationships between Al_2O_3 and Fe_2O_3 (Fig. 4b) show that the soil samples of these three profiles and their underlying bedrocks have a good positive correlation ($R^2 = 0.88$), similar to that between Al_2O_3 and TiO_2. Further, the DFY soil profile and DFYB rock samples show no obvious correlation between Al_2O_3 and Fe_2O_3. The rock samples have relatively higher contents of these immobile elements, probably due to the loss of highly

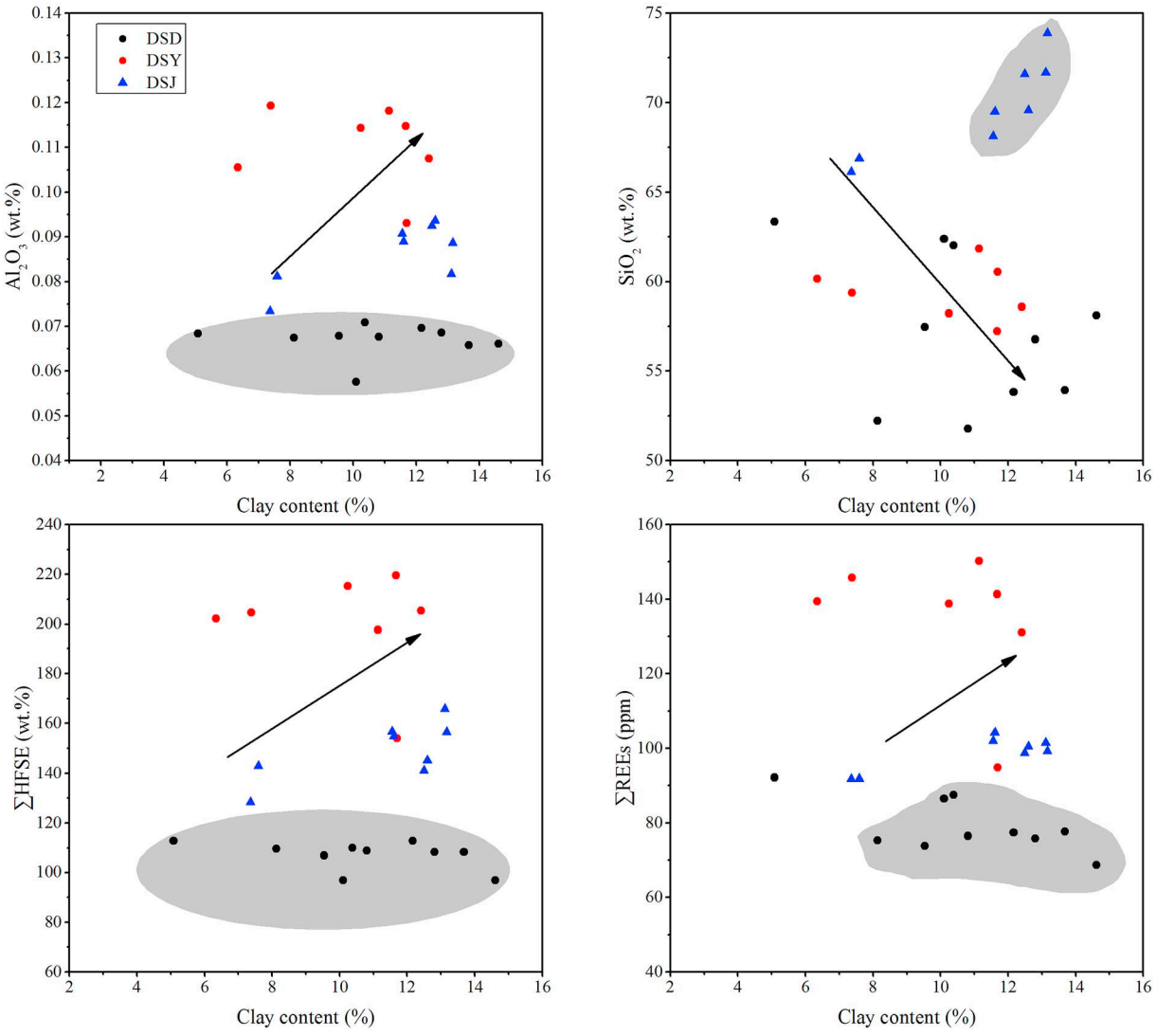

Fig. 3. Plot of Al_2O_3, SiO_2, HFSE and REEs concentrations vs. clay content for bulk samples in the DSD, DSY, DSJ soil profiles.

mobile elements such as alkalis and alkali earth elements in the formation process (Gu et al., 2013). The samples have relatively smaller correlations between Fe_2O_3 and Al_2O_3 than between TiO_2 and Al_2O_3, possibly because Fe in the Fe(II) form is relatively mobile (Muhs et al., 2013). The trend of Al accumulation in DFY and DFYB samples are most likely due to the retention of clay and Al-rich minerals, respectively. In addition to these immobile elements, there are good correlations between MnO_2, Fe_2O_3, K_2O, MgO and TiO_2 (Supplementary Fig. 5), suggesting a similarity in host minerals between different profile samples. The above characteristics indicate that the three profile soils are possibly the in situ or quasi-in situ products of the underlying substrates (carbonaceous shale and dolomite limestone), and they possibly have a cognate relationship. However, it is difficult to distinguish between the soils developed on shale and carbonatite within this small region.

As shown in Supplementary Fig. 1, the DSD profile soil has lower CIA values and that some DSJ samples have the same CIA values as DSY samples with the same K_2O, MgO and TiO_2 contents, while other DSJ samples seem to resemble other profile samples. As shown in Fig. 4, DSJ samples are distributed widely relative to DSD and DSY samples. From the perspective of geomorphology, the DSY and DSJ profiles, which are located at the lower positions on this hillslope, cannot remain undisturbed or uneroded. Muhs and Budahn (2009) also struggled to find undisturbed or uneroded soil profiles on the lower terraces along the north coast of Jamaica. To compare possible soil sources, we employ plots of SiO_2/Al_2O_3 vs. K_2O/Al_2O_3, following Ji et al. (2004) and Wei et al. (2013) (Fig. 5). The SiO_2/Al_2O_3 ratios and K_2O/Al_2O_3 ratios of DSD, DSY and DSJ soil samples are consistent and only slightly variable (~10 and 0.1, respectively). In addition, samples from the above three profiles are all concentrated in a relatively small region, which is far away from that of the DFYB samples. The major element data indicate that the DSD, DSY and DSJ soil profiles act as a whole, although they have different types of bedrock. Meanwhile, due to the different topographical features of the profiles driving soil erosion, the behaviors of elements during chemical weathering may be different in various hillslope positions.

As similar crustal incompatible elements, Zr and Hf can be used to distinguish different crustal processes (Hu and Yang, 2016). The ratios of crustal incompatible elements, such as the Zr/Hf ratio, in soil profiles and bauxite can be employed to identify parent materials (Calagari and Abedini, 2007). When plotted in a cross plot, the ratios of crustal incompatible elements can generate highly correlated liner arrays that are consistent through to the origin of the plot, which is a part of the parent materials (MacLean, 1990). The concentrations of Hf and Nb in all three profile samples (including their bedrocks) are significantly correlated with the concentrations of Zr and Ta, respectively (Fig. 6), also indicating that the soils and the bedrocks have a cognate relationship.

The geochemical tracer methods discussed above show that the three soil profiles were possibly derived from the underlying bedrock.

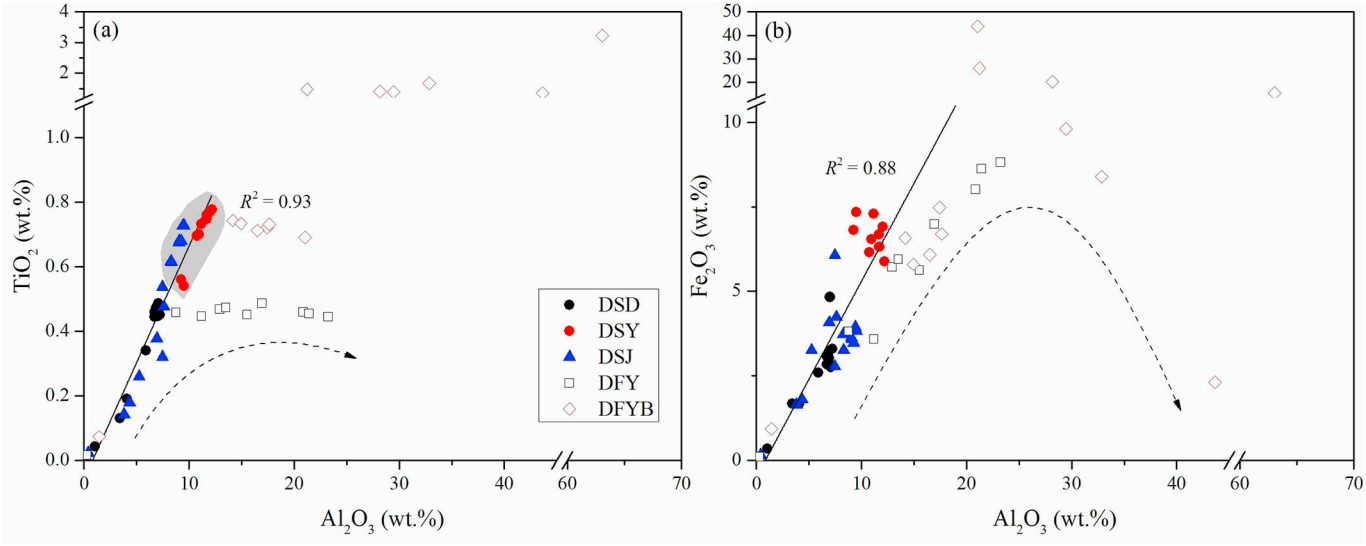

Fig. 4. (a) Distribution of TiO_2 and Al_2O_3 in bulk samples from the DSD, DSY, DSJ DFY profile samples and DFYB rock samples. (b) Distribution of Fe_2O_3 and Al_2O_3 in bulk samples from the DSD, DSY, DSJ and DFY profile samples and DFYB rock samples.

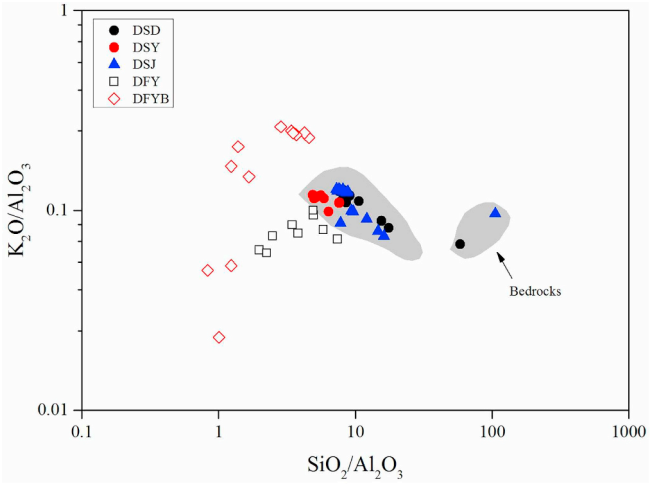

Fig. 5. Plot of K_2O/Al_2O_3 vs. SiO_2/Al_2O_3 for bulk samples in the DSD, DSY, DSJ, DFY soil profiles and DFYB rock samples.

Although the underlying carbonaceous shale and dolomite limestone provide the weathering products directly for DSD, and DSY and DSJ, the topographic features and inconsistency of bedrock lithology also play a nonnegligible role in soil genesis in this area. Furthermore, we found no correlation between the soil in this area and the eolian source related to the Emeishan basalt, indicating that this component is not a major material source. The data show that there is a close affinity among these three profile soils, which indicates that the three profile soils have similar material. Topographical features (e.g., slope, soil thickness) have been suggested to influence the inheritance relationships of the topsoil in the three profiles through physical erosion and sedimentation, and this point is consistent with the data discussed above. Although we cannot rule out the possibility of input from other sources, the above geochemical characteristics indicate that the three profile soils are possibly the in situ of the underlying shale and carbonatite substrates. Many scholars proposed that the soils of karst regions in southwestern China are the in situ products of the underlying carbonatite substrates (Ji et al., 2004; Wei et al., 2013). Although two types of bedrock are present in this studied hillslope resulting in difficulty to distinguish

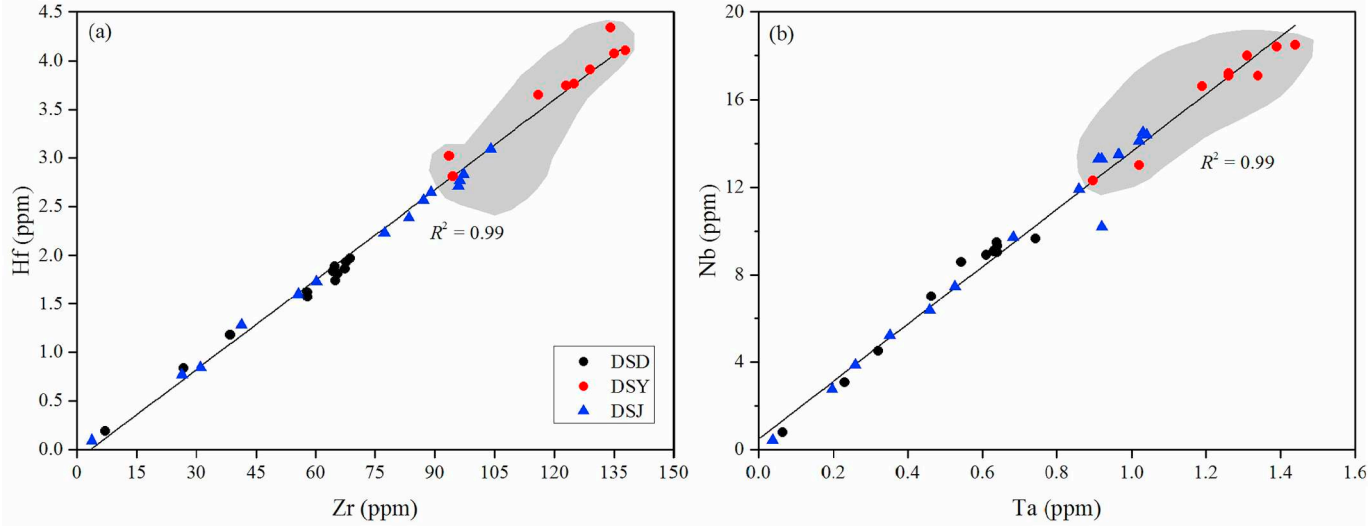

Fig. 6. (a) Hf vs. Zr concentrations, (b) Nb vs. Ta concentrations for the DSD, DSY and DSJ soil profiles.

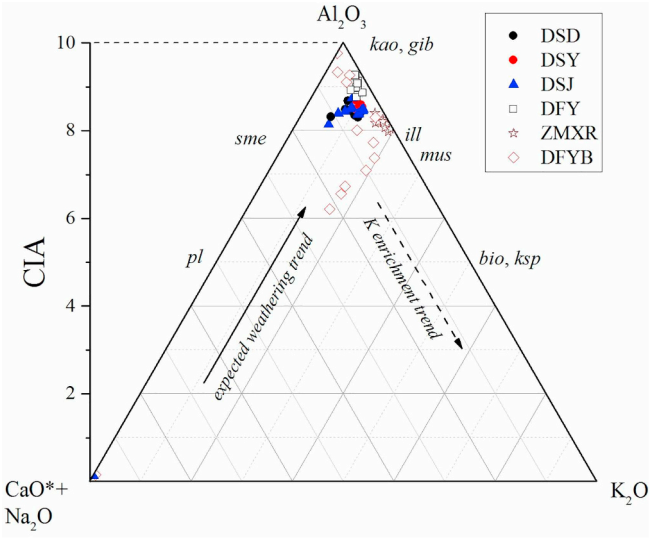

Fig. 7. A-CN-K diagram of the DSD, DSY, DSJ, DFY, ZMXR soil profiles and DFYB rock samples.

each profile provenance, while we insist that the weathering products of the underlying carbonatite are the main source of these profiles which overlying carbonatite substrates. Considering the soil erosion characteristics of the hillslope, we suggest that the soil source of deposition area on karst hillslopes could be influenced by the input of soil from upslope via soil erosion.

4.4. Element geochemical behaviors in soil formation

4.4.1. Major element behaviors in soil formation

A-CN-K ternary diagrams portray the molar proportions of the molar ratios of Al_2O_3 (A apex), CaO* + Na_2O (CN apex) and K_2O (K apex) for the bulk soil samples (Fig. 7), which have empirically and kinetically predictable weathering vectors for in situ weathering profiles (Fedo et al., 1995; Nesbitt and Young, 1984; Nesbitt and Young, 1989). The CaO contained in phosphorite and carbonate minerals should be deducted from the total CaO content before drawing such a diagram of molar ratio. Here, we deducted calcium carbonate content in carbonate minerals. As shown in Fig. 7, the overall weathering vector of the DFYB rock samples is parallel or subparallel to the A–CN axis and then tends to the A apex, reflecting a process in which CaO* + Na_2O and K_2O are leached out and Al_2O_3 is increased in these samples. All three soil profiles (DSD, DSY and DSJ) are distributed along the A–CN axis and show enrichment in K. The enrichments in K in the ZMXR and DFY soil samples are significant and are attributed to preferential adsorption on clay minerals due to the larger ionic radius of K than those of Na and other elements, which more easily remain in solution during the weathering process (Panahi et al., 2000). The overall weathering vector of all soil samples indicates the significant destruction of feldspar (albite and anorthite) especially in the DSY profile, indicating the strong chemical weathering during incipient pedogenesis process. Considering the topographic feature of soil thickness, the shallower soil favors feldspar dissolution (Jin et al., 2010). Furthermore, this weathering trend leads to higher CIA and chemical index of weathering (CIW) values in DSY soils than in DSD and DSJ soils.

Scholars have proposed many behavior patterns for major elements during chemical weathering, such as "the decrease in SiO_2 and constancy in TiO_2," "the decrease in SiO_2 and increase in Al_2O_3" and "the decrease in K_2O and increase in Al_2O_3" (Ji et al., 2004). Fig. 8 shows the concentrations of SiO_2, Al_2O_3, TiO_2 and K_2O with sampling depth in the DSD, DSY, DSJ and DFY profiles. As stated above, these four profile soils do not display "the decrease in K_2O" pattern. In the undisturbed profile (DFY), the SiO_2 contents decrease while Al_2O_3, TiO_2 and K_2O contents increase from the lowest soil sample to the upper soils during the weathering process. Similar results are observed for the DSD and DSY soil profiles. In the toeslope profile (DSJ profile), the behavior of SiO_2 is different from those in the DSD, DSY and DFY profiles, which decrease from the lowest soil sample to the upper soils during weathering. Comparing the other profiles with the undisturbed profile (DFY profile), we suggest that the weathering trends of the DSD and DSY profiles are normal and that the "the decrease in SiO_2 and increase in TiO_2," "the decrease in SiO_2 and increase in Al_2O_3" and "the decrease in SiO_2 and increase in K_2O" are ubiquitous in this study area. Feldspar constitute a fair amount of Si is and the rest incorporated in quartz (resistant to chemical weathering), leading to a loss of Si by both soluble and particle loads. As shown in Table 2, the clay contents (%) of the DSJ upper profile is less than that of the DSD and DSY profile. Usually, the fine soil particles have less SiO_2 content, due to reducing of quartz and feldspar concentrations. Considering the topography of the hillslope, coarse particles from the upper slope could be transported and accumulated in the lower region (toeslope) (Anderson et al., 2002; Jin et al., 2010), while the fine particles (such as clay minerals) loss via soil migration, resulting in the abnormal behavior of Si in DSJ soils.

4.4.2. High field strength element behaviors in soil formation

In any case, the high field strength elements (HFSEs) are found in highly resistant minerals (such as Zr and Hf in zircon) hence are suitable to address the issues concerning the sources of materials for sedimentary rocks, terra rossa, loess and deep-sea sediments (Gu et al., 2013; Hu and Yang, 2016; McLennan, 1989; Muhs and Budahn, 2009; Muhs et al., 2007; Olivarez et al., 1991). In addition to this application, the high field strength elements can also be used to trace transport paths due to their reduced solution and physical migration.

As shown in Fig. 6, there are significantly positive correlations between Zr and Hf (R^2 = 0.99) and between Nb and Ta (R^2 = 0.99), indicating that these elements have a cognate relationship. As stated above, DSY soils have higher CIA and CIW values. From bedrock to profile soils, the contents of Zr, Hf, Nb and Ta increase with chemical weathering intensity, which indicates that these elements are highly stable in the process of supergene weathering (Wei et al., 2013). While the upper soils of DSJ (dashed area in Fig. 6) have concentrations similar to those of the DSY samples, the best explanation is probably that DSJ topsoil has an allochthonous origin by soil erosion from the upslope site (such as the DSY profile). In karst region, the distribution and behavior of trace elements could be influenced by clay mineral adsorption, soil pH values, organic matter adsorption (Liu, 2009). As stated above, the DSJ upper profile acquired accumulation of coarse particles due to transport from upslope (such as the DSY), resulting in the relative lower contents of Zr, Hf, Nb and Ta elements in the DSJ topsoil. The coarse particles contain less organic matters, which also account for the low contents of these four trace elements. The acid environment enhances the decomposition of the primary minerals, and organic matter may form organic colloids which significantly improve the transportation of insoluble elements such as Ti, Zr, and Th in aqueous solution (Ma et al., 2007). The acid environment (low pH values) of the DSD profile enhances the transportation of these trace elements, resulting in the lower contents.

Th is a stable element in almost all soil profiles, while chemical leaching may result in the output of U from weathered soil profiles (i.e., insoluble U^{4+} can be oxidized to soluble U^{6+} by weathering process). Hence, Th/U ratios tend to decrease in soil profiles (Ji et al., 2004). As the weathering degree increases, the U/Th ratios decrease from bedrock to DSY soils (Supplementary Fig. 5). DSY soils and the topsoils of the DSJ profile have the highest Th contents and constant U/Th ratios within a certain range. This result illustrates that Th is hosted in heavy immobile minerals, which resist chemical weathering, and that U could be lost from soils during profile formation.

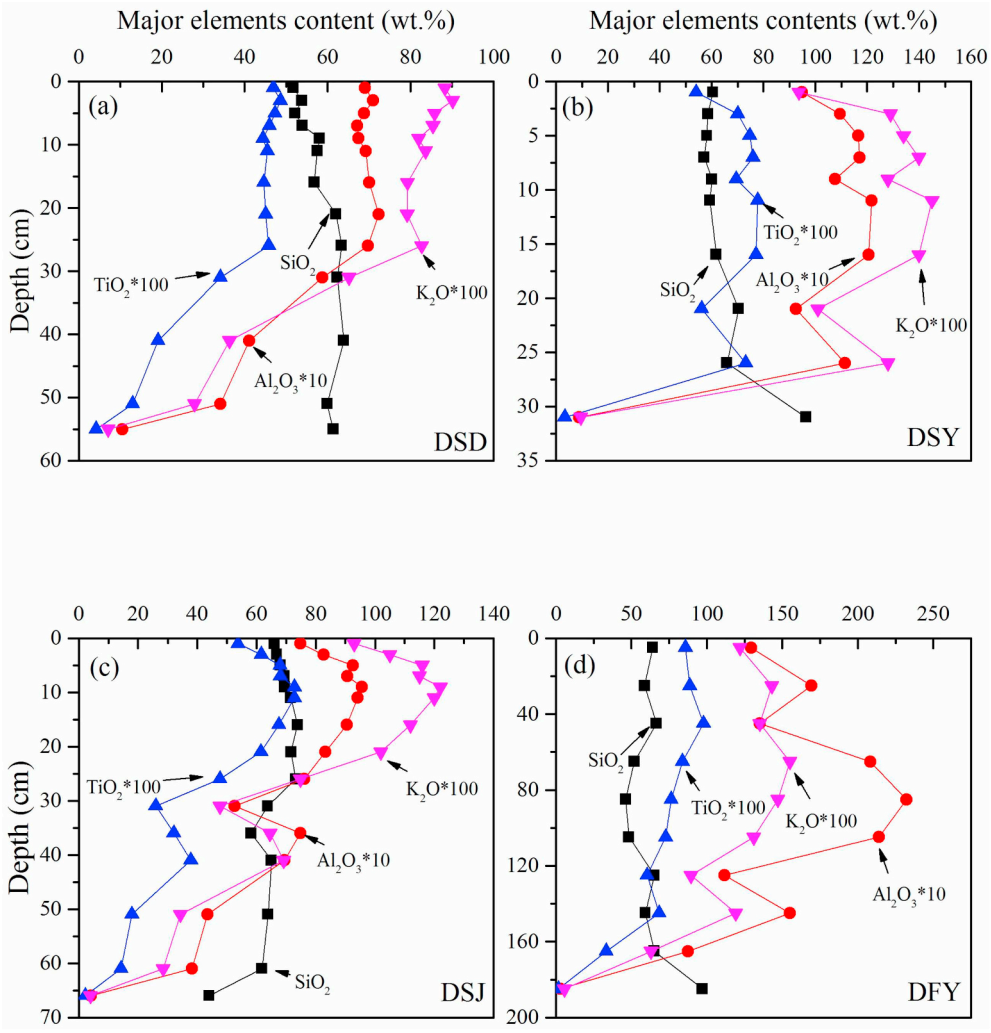

Fig. 8. The concentrations of SiO_2, Al_2O_3, TiO_2 and K_2O with sampling depth in the DSD, DSY, DSJ and DFY profiles.

4.4.3. REE behaviors in soil formation

REEs tend to be mobile and to undergo fractionation during chemical weathering processes (Babechuk et al., 2014; Laveuf and Cornu, 2009). $\tau_{Ti,\ REE}$, $\tau_{Ti,\ Al}$, LOI, Fe_2O_3(T) vs. FeO contents, $\tau_{Ti,\ Mn}$ and P_2O_5 contents in the DSD, DSY and DSJ profile soils are shown in Fig. 9. All of the DSD and DSJ profiles show negative values for REEs, and most of these values decrease towards the surface (Fig. 9a, c), which is consistent with the loss of REEs towards the surface (Ma et al., 2011b). As demonstrated above, the $\tau_{Ti,\ j}$ values for both LREEs and HREEs change dramatically in the lower parts (26–51 cm and 31–61 cm) of DSD and DSJ profiles and change minimally in the upper parts. Meanwhile, unlike the smooth depletion trends shown for DSD and DSJ profiles, the DSY profile shows "zig-zag" patterns with inconsistent trends in the $\tau_{Ti,\ REE}$ values. Overall, the DSY profile experienced less REE loss than the DSD and DSJ profiles. The $\tau_{Ti,\ j}$ values of LREEs and HREEs in the DSJ profile are similar and are approximately −0.9 in the upper part. The $\tau_{Ti,\ j}$ values of La, Pr and Nd in the DSD profile reach approximately −0.3, but the $\tau_{Ti,\ j}$ values of Sm, Eu and Gd are similar to the $\tau_{Ti,\ j}$ of HREEs and equal approximately −0.6 in the upper part, showing more depletion in the middle REEs (MREEs) and HREEs than in the LREEs.

The ability of REEs to absorb onto mineral surface, especially Mn-Fe hydroxides, secondary phosphate minerals and clay minerals, determines their adsorption in soils (Braun et al., 2017; Jin et al., 2017; Su et al., 2017). In Fig. 10, there are significantly positive correlations between REEs and Al_2O_3, REEs and Fe_2O_3, REEs and MnO and REEs and P_2O_5. These results are consistent with the observation in these samples at the sampling depth (shaded band in Fig. 9). The positive correlation between the REE-Ce and Al_2O_3 in all three profile soils is the most significant (R^2 = 0.902), implying that the clay minerals are the most common host of REEs in all soil samples. This result suggests that the REE-Ce could physically migrate along with clay minerals. Overall, the Mn-Fe hydroxides and secondary phosphate minerals also have a significant effect on the mobility of REE-Ce, especially in the DSD profile (R^2 = 0.932 between REE-Ce and MnO). Considering the erosion situation and vegetation coverage in the DSD profile (deposition profile), the REE-Ce in the DSD profile could be transported by chemical migration via soil solution. Similar to the high field strength elements, the transport of REEs can be significantly enhanced by low pH value and high organic matter content (Braun et al., 2017). As shown in Table 2, the DSD profile soils have lowest pH values, which are influenced by the overlying vegetation, and in general have more organic matters than the DSY and DSJ profiles, resulting in the vertical transport of REEs and the lateral migration with organic colloids via soil solution. This may explain the high $\tau_{Ti,\ REE}$ values and the lowest REEs content (as shown in Table 5 and Fig. 10) of the DSD profile relative to other two profiles especially for the DSY profile. Jin et al. (2010) suggested that the less soluble elements such as Al and Fe are lost predominantly through subsurface transport of particles larger than 1.3 μm, i.e. particles that were filtered out by the suction lysimeters. During chemical weathering, REEs usually released into solution and are adsorbed onto fine particles (such as clay), then subsequently transported along with the fine particles. The loss of fine particles in the DSJ topsoil could

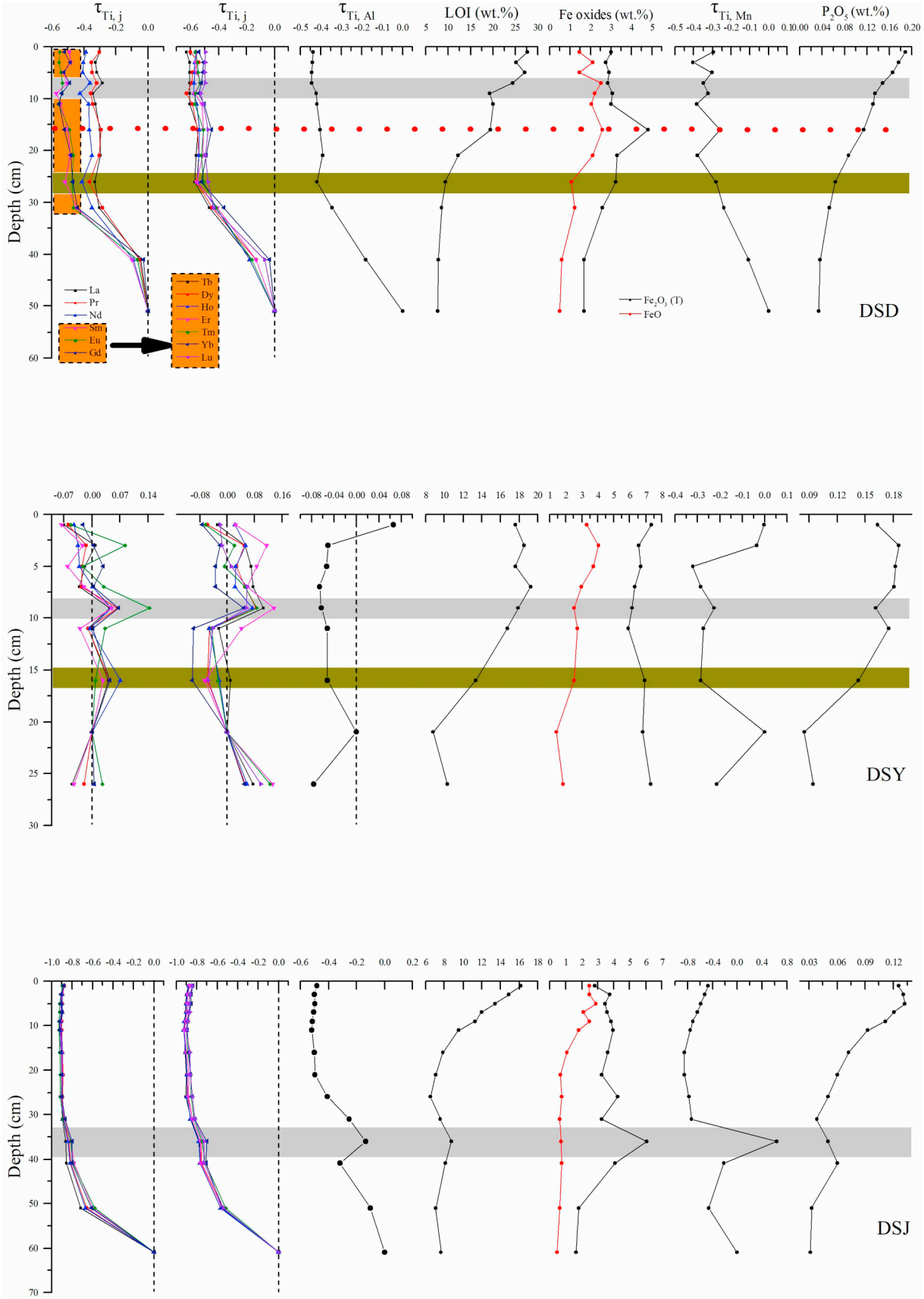

Fig. 9. Depth variations of $\tau_{Ti,\ REE}$, $\tau_{Ti,\ Al}$, LOI, Fe_2O_3(T) vs. FeO contents, $\tau_{Ti,\ Mn}$ and P_2O_5 contents in the DSD, DSY and DSJ profile soils.

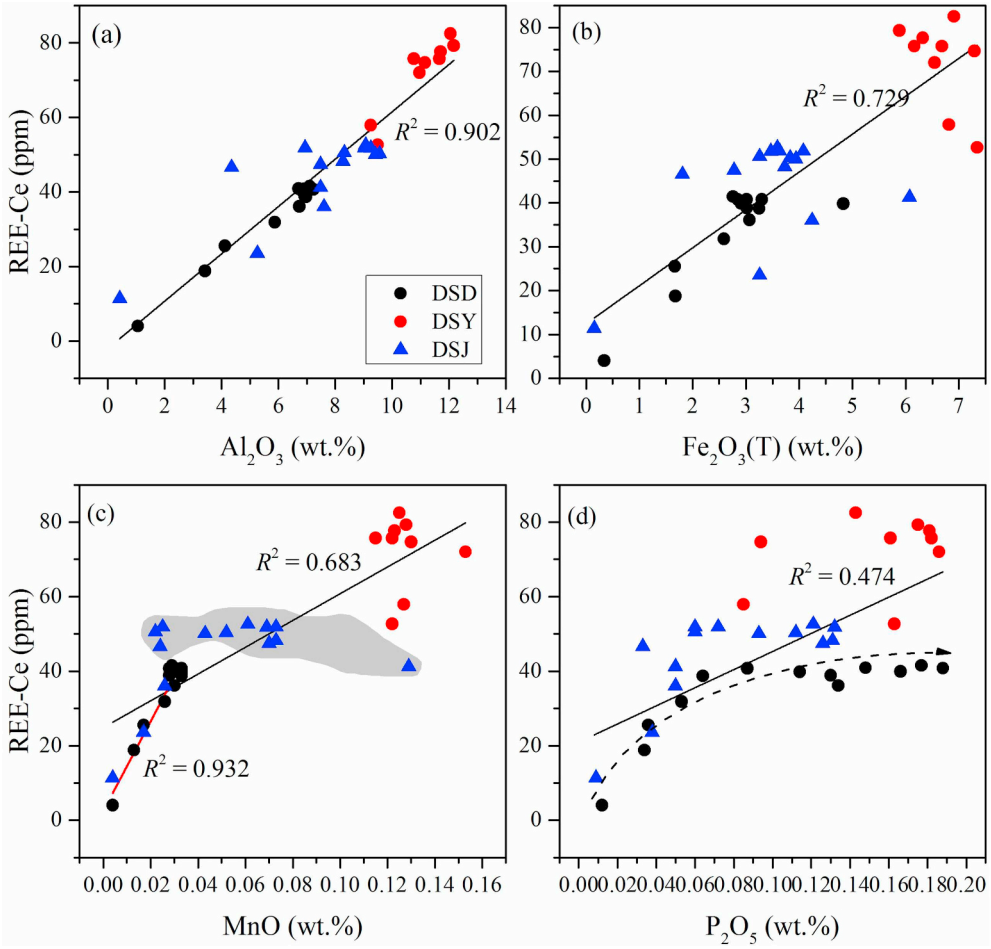

Fig. 10. The relationship between the REE-Ce concentrations (mean value of total rare earth element contents minus concentration of element Ce) and oxides Al_2O_3 (a), Fe_2O_3 (b), MnO (c), and P_2O_5 (d) for the DSD, DSY and DSJ profile samples.

account for the low contents of REEs. The DSJ profile (toeslope) with the greatest slope (28.89°) was due to the construction of road which could lead to migration of REEs via soil solution in the middle and low section of the DSJ profile, which have higher clay contents than the DSY profile. The topographical features and soil properties of the DSJ profile jointly lead to the low REEs contents and high $\tau_{Ti,\ REE}$ values relative to the DSY profile.

4.5. Effects of soil erosion on chemical weathering

The three soil profiles show patterns in HFSEs similar to those in REEs (discussed above) relative to soil erosion characteristics (Fig. 11b). Unlike elements Al and Fe, the U and Th mass balance at the Susquehanna/Shale Hills Observatory (SSHO) also requires that both U and Th are lost due to solutes and particles from weathering soils during chemical weathering processes (Jin et al., 2010). Moreover, the acidic and organic materials present in DSD soils could also enhance the mobility of insert elements, such as Al and Th (Braun et al., 2005). We propose that the HFSEs in DSD soils are mainly lost as solutes through chemical migration and are depleted in DSY and DSJ soils along with particles by physical migration.

As shown in Fig. 11c, there is a significantly negative correlation between REE-Ce and ^{137}Cs activity ($R^2 = -0.809$) in DSY soils. The ^{137}Cs activity increases towards the topsoil in all three profiles, as shown in Fig. 2. The deposited ^{137}Cs adsorbed by fine soil particles and humic acid is resistant to chemical or biological weathering (Rahimi et al., 2013; Song et al., 2018; Zapata, 2002). This result could be due to the presence of thin soil layer and relative low clay contents in the DSY profile, which lead to REEs transferred downwards easier via soil solution, while ^{137}Cs is resistant to chemical or biological removal. In the DSJ samples, the REE-Ce contents are parallel to the axis of ^{137}Cs activity, suggesting that the topsoil of the DSJ profile supplied from the DSY profile loses REEs via clay contents loss (as discussed above) and secondary chemical weathering which occurred in an open environment (Anderson et al., 2002), leading to lower contents of REEs than those found in DSY soils. In the DSD profiles, the REE-Ce contents are also parallel to the axis of ^{137}Cs activity. The erosion characteristic in the DSD profile (no soil erosion) obviously implies that the depletion of REEs in DSD soils occurs in soil water by chemical migration, and the low pH values enhances REEs transport downwards within profile as a result no relationship between the REE-Ce contents and ^{137}Cs activity. The migration patterns of HFSEs are similar to those of REE migration and are shown in Fig. 11d. The HFSEs of DSD soil experience obvious chemical migration by solutes. The disturbed profiles (DSY and DSJ profiles) lose HFSEs along with host particles by physical migration.

As discussed above, all four soil profiles (DSD, DSY, DSJ and DFY) display K enrichment. The CIA, which is sensitive to potassium metasomatism, may not be suitable for showing the chemical weathering intensity of these soils. However, the CIW is not affected by K enrichment. The CIA is also calculated based on the average composition of Na and Ca in natural silicate minerals and the molar ratio of CaO/Na_2O in the soil sample, assuming that for CaO* the molar CaO/Na_2O ratio of silicates is not > 1. If this ratio is < 1, the CIA is calculated directly from the molar content of CaO, which is equivalent to m CaO* = m

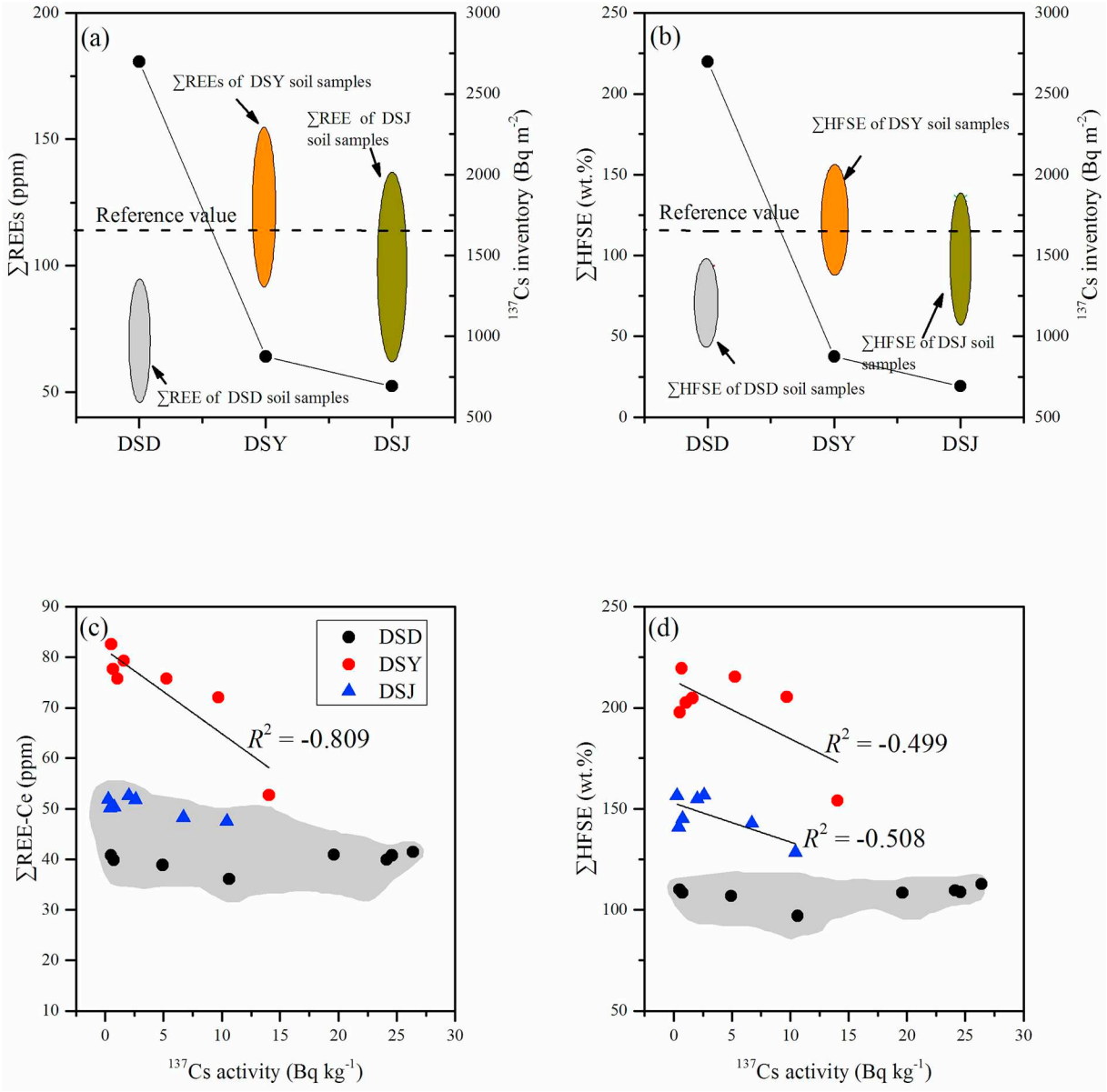

Fig. 11. (a) ^{137}Cs inventories and the concentrations of REE, (b) ^{137}Cs inventories and the concentrations of HFSE in DSD, DSY and DSJ soil samples. The relationship between the ^{137}Cs activities and ΣREE-Ce concentrations (mean value of total rare earth element contents minus concentration of element Ce) (c) and HFSE concentrations (d) for DSD, DSY and DSJ soil samples.

CaO. On the other cases, the CaO content of silicates is supposed to be equivalent to the Na_2O content. In Fig. 12, the CIA and CIW values of soils are shown against the sampling depth. Clearly, the CIA and CIW values of DSY samples are higher than those of all other soil samples from the DSD and DSJ profiles (excluding the upper 5 samples of the DSJ profile). Considering the erosion characteristics, the DSY and DSJ profiles experienced significant soil erosion. The topsoil of the DSY profile might be transported to the DSJ profile due to soil erosion, leading to the high CIW values of the upper 5 soil samples of the DSJ profile. Because of the reduced depletion of HFSEs and REEs in DSY soils, we suggest that significant soil erosion may lead to the high intensity of chemical weathering and that feldspar (albite and anorthite) may be preferentially weathered. Jin et al. (2010) stated that shallow bedrock (thinner soil) initially leads to the dissolution of feldspar, followed by the dissolution of clay minerals in the soil. This process could explain why DSY soils have higher CIW and CIA values and lower depletions in REEs and HFSEs. There is less mass loss as a result of chemical weathering in the deposition area than in the erosion area (Yoo et al., 2009). To some extent, this is unusual as there are more minerals in the area of deposition (due to accumulation of thick soils) which react with rich soil water. In the DSD profile (deposition profile), the soils have the lowest concentrations of REEs and HFSEs, implying that their loss is mainly due to chemical leaching rather than transport with particles by physical erosion. Considering the topographic feature, the DSJ profile has the highest soil erosion rate, while this profile could receive the soil transported by erosion from the DSY profile. Therefore, we propose that the fresh soil from the DSY profile could limit the in situ chemical weathering, although it experiences significant soil erosion. Anderson et al. (2002) proposed that thicker soil could reduce chemical weathering rates, because more clay minerals prevent the infiltration of surface water. This effect can also explain the lower CIA and CIW values in DSD and DSJ soils. Above all, we believe that at some intermediate soil erosion rate, that soils without the input of fresh materials could experience the strongest chemical weathering, resulting in vast dissolution of minerals (such as feldspar).

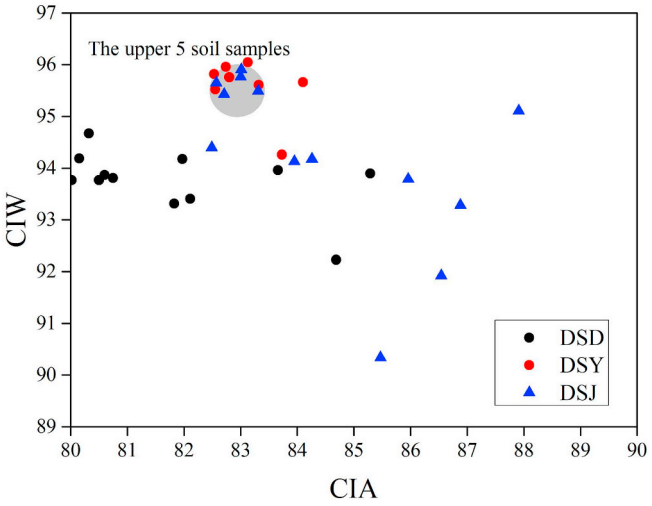

Fig. 12. Correlations between the chemical index of alteration (CIA) and chemical index of weathering (CIW) values of DSD, DSY and DSJ soil samples.

5. Conclusions

The soil redistribution rates for this studied hillslope were found to be 11.88, −15.31 and −21.03 t ha^{-1} year^{-1} at the summit, shoulder and toeslope respectively. This result using ^{137}Cs measurement highlight severe soil erosion associated in this studied hillslope in Nanchuan County, southwest China. The study further illustrate that the effects of human activities such as the construction of roads, mining and deforestation, can significantly accelerate the rate of soil erosion, especially in the toeslope component with rare vegetation coverage. Therefore, the study of chemical weathering and soil formation in this area should not ignore the effect of soil erosion coupled with topographic features.

Major and trace element data indicate that the summit (DSD), shoulder (DSY) and toeslope (DSJ) profile soils of this studied hillslope are possibly the in situ products of the underlying substrates. Furthermore, the topographical features and inconsistency of bedrock lithology play a nonnegligible role in soil genesis in this small region. Although the hillslope soils are influenced by the topographic features and inconsistent bedrock lithology, we insist that the weathering products in this area are mainly of carbonate source, which is derived from the overlying carbonatite substrates.

The Al, rare earth elements (REEs) and high field strength elements (HFSEs) contents increase with increasing clay content in DSY and DSJ profiles, indicating that these elements could be loss with clay particles via soil erosion. The coarse particles accumulation and fine particles (such as clay minerals) loss result in the enrichment of Si in erosion profile surface (DSJ profile). The DSD profile (deposition profile) soils with low pH values and high clay contents have the lowest concentrations of REEs and HFSEs, implying that their loss is mainly due to chemical leaching rather than by transport with particles and physical erosion.

Considering the topographical features, the DSJ profile has the highest soil erosion rate, while it could receive the soil transported by erosion from the DSY profile. Therefore, we propose that the fresh soil from the DSY profile could limit the in situ chemical weathering, although DSJ experiences significant soil erosion. Above all, we believe that at some intermediate soil erosion rate, that soils without the input of fresh materials could experience the strongest chemical weathering, resulting in vast dissolution of minerals (such as feldspar). The soil texture, topographical features, vegetation coverage and human activities together affect the soil chemical weathering, physical erosion and element behaviors in karst hillslope.

Supplementary data to this article can be found online at https://doi.org/10.1016/j.catena.2019.104133.

Acknowledgements

This work was supported by the National Natural Science Foundation of China (NSFC) grants (41473122, 41073096, 41473027), the National Key Basic Research Program of China, China (2013CB956702) and the Hundred Talents Program of the Chinese Academy of Sciences.

References

Acosta, J.A., Martínez-Martínez, S., Faz, A., Arocena, J., 2011. Accumulations of major and trace elements in particle size fractions of soils on eight different parent materials. Geoderma 161, 30–42.
Anderson, S.P., Dietrich, W.E., Brimhall, G.H., 2002. Weathering profiles, mass-balance analysis, and rates of solute loss: linkages between weathering and erosion in a small. steep catchment. Geol. Soc. Am. Bull. 114, 1143–1158.
Ayoubi, S., Ahmadi, M., Abdi, M.R., Abbaszadeh Afshar, F., 2012. Relationships of 137Cs inventory with magnetic measures of calcareous soils of hilly region in Iran. J. Environ. Radioact. 112, 45–51.
Babechuk, M.G., Widdowson, M., Kamber, B.S., 2014. Quantifying chemical weathering intensity and trace element release from two contrasting basalt profiles, Deccan Traps, India. Chem. Geol. 363, 56–75.
Brantley, S.L., Goldhaber, M.B., Ragnarsdottir, K.V., 2007. Crossing disciplines and scales to understand the critical zone. Elements 3, 307–314.
Braun, J.J., Ngoupayou, J.R.N., Viers, J., Dupre, B., Bedimo, J.P.B., Boeglin, J.L., Robain, H., Nyeck, B., Freydier, R., Nkamdjou, L.S., Rouiller, J., Muller, J., 2005. Present weathering rates in a humid tropical watershed: Nsimi, South Cameroon. Geochim. Cosmochim. Acta 69, 357–387.
Braun, J.J., Marechal, J.C., Riotte, J., Boeglin, J.L., Bedimo Bedimo, J.P., Ndam Ngoupayou, J.R., Brunot, Robain, H., Sekhar, M., Audry, S., Viers, J., 2012. Elemental weathering fluxes and saprolite production rate in a Central African lateritic terrain (Nsimi, South Cameroon). Geochim. Cosmochim. Acta, 99, 243–270.
Braun, J.J., Riotte, J., Battacharya, S., Violette, A., Prunier, J., Bouvier, V., Candaudap, F., Maréchal, J.C., Ruiz, L., Panda, S.R., Subramanian, S., 2017. REY-Th-U solute dynamics in the critical zone: combined influence of chemical weathering, atmospheric deposit leaching, and vegetation cycling (Mule Hole Watershed, South India). Geochem. Geophys. Geosyst. 18, 4409–4425.
Brimhall, G.H., Dietrich, W.E., 1987. Constitutive mass balance relations between chemical composition, volume, density, porosity, and strain in metasomatic hydrochemical systems: results on weathering and pedogenesis. Geochim. Cosmochim. Acta 51, 567–587.
Bruun, T.B., Elberling, B., Christensen, B.T., 2010. Lability of soil organic carbon in tropical soils with different clay minerals. Soil Biol. Biochem. 42, 888–895.
Calagari, A.A., Abedini, A., 2007. Geochemical investigations on Permo-Triassic bauxite horizon at Kanisheeteh, east of Bukan, West-Azarbaidjan, Iran. J. Geochem. Explor. 94, 1–18.
Fedo, C.M., Nesbitt, H.W., Young, G.M., 1995. Unraveling the effects of potassium metasomatism in sedimentary rocks and paleosols, with implications for paleoweathering conditions and provenance. Geology 23, 921–924.
Feng, T., Chen, H.G., Polyakov, V.O., Wang, K.L., Zhang, X.B., Zhang, W., 2016. Soil erosion rates in two karst peak-cluster depression basins of northwest Guangxi, China: comparison of the RUSLE model with ^{137}Cs measurements. Geomorphology 253, 217–224.
Fernández, C., Vega, J.A., 2016. Evaluation of RUSLE and PESERA models for predicting soil erosion losses in the first year after wildfire in NW Spain. Geoderma 273, 64–72.
Ge, N.N., Wei, X.R., Wang, X., Liu, X.T., Shao, M.G., Jia, X.X., Li, X.Z., Zhang, Q.Y., 2019. Soil texture determines the distribution of aggregate-associated carbon, nitrogen and phosphorous under two contrasting land use types in the Loess Plateau. Catena 172, 148–157.
Gong, Q.J., Deng, J., Yang, L.Q., Zhang, J., Wang, Q.F., Zhang, G.X., 2011. Behavior of major and trace elements during weathering of sericite–quartz schist. J. Asian Earth Sci. 42, 1–13.
Gu, J., Huang, Z.L., Fan, H.P., Jin, Z.G., Yan, Z.F., Zhang, J.W., 2013. Mineralogy, geochemistry, and genesis of lateritic bauxite deposits in the Wuchuan–Zheng'an–Daozhen area, Northern Guizhou Province, China. J. Geochem. Explor. 130, 44–59.
Guo, Q.K., Hao, Y.F., Liu, B.Y., 2015. Rates of soil erosion in China: a study based on runoff plot data. Catena 124, 68–76.
Harnois, L., 1988. The CIW index: a new chemical index of weathering. Sediment. Geol. 55, 319–322.
Hu, F.G., Yang, X.P., 2016. Geochemical and geomorphological evidence for the provenance of aeolian deposits in the Badain Jaran Desert, northwestern China. Quat. Sci. Rev. 131, 179–192.
Ji, H.B., Wang, S.J., Ouyang, Z.Y., Zhang, S., Sun, C.X., Liu, X.M., Zhou, D.Q., 2004. Geochemistry of red residua underlying dolomites in karst terrains of Yunnan-Guizhou Plateau: I. The formation of the Pingba profile. Chem. Geol. 203, 1–27.
Jin, L.X., Ravella, R., Ketchum, B., Bierman, P.R., Heaney, P., White, T., Brantley, S.L., 2010. Mineral weathering and elemental transport during hillslope evolution at the Susquehanna/Shale Hills Critical Zone Observatory. Geochim. Cosmochim. Acta 74, 3669–3691.
Jin, L.X., Ma, L., Dere, A., White, T., Mathur, R., Brantley, S.L., 2017. REE mobility and fractionation during shale weathering along a climate gradient. Chem. Geol. 466, 352–379.

Jungers, M.C., Bierman, P.R., Matmon, A., Nichols, K., Larsen, J., Finkel, R., 2009. Tracing hillslope sediment production and transport with in situ and meteoric10Be. J. Geophys. Res. 114.
Laveuf, C., Cornu, S., 2009. A review on the potentiality of Rare Earth Elements to trace pedogenetic processes. Geoderma 154, 1–12.
Li, H., Zhang, X.B., Wang, K.L., Wen, A.B., 2009. ^{137}Cs distribution characteristics at a talus-type karst slope in northwestern Guangxi. J. Soil Water Conserv. 23, 42–47.
Lin, D.Y., 2002. Soil Science. China Forestry Publishing House, Beijing.
Liu, C.Q., 2009. Biogeochemical Processes and Cycling of Nutrients in the Earth's Surface: Cycling of Nutrients in Soil-Plant Systems of Karstic Environments, Southwest China. Science Press, Beijing.
Lü, Y.W., Gu, Z.Y., Aldahan, A., Zhang, H.C., Possnert, G., Lei, G.L., 2010. ^{10}Be in quartz gravel from the Gobi Desert and evolutionary history of alluvial sedimentation in the Ejina Basin, Inner Mongolia, China. Chin. Sci. Bull. 55, 3802–3809.
Lucke, B., Kemnitz, H., Bäumler, R., Schmidt, M., 2014. Red Mediterranean soils in Jordan: new insights in their origin, genesis, and role as environmental archives. Catena 112, 4–24.
Ma, J.L., Wei, G.J., Xu, Y.G., Long, W.G., Sun, W.D., 2007. Mobilization and re-distribution of major and trace elements during extreme weathering of basalt in Hainan Island, South China. Geochim. Cosmochim. Acta 71, 3223–3237.
Ma, L., Jin, L.X., Brantley, S.L., 2011a. Geochemical behaviors of different element groups during shale weathering at the Susquehanna/Shale Hills Critical Zone Observatory. Appl. Geochem. 26, S89–S93.
Ma, L., Jin, L.X., Brantley, S.L., 2011b. How mineralogy and slope aspect affect REE release and fractionation during shale weathering in the Susquehanna/Shale Hills Critical Zone Observatory. Chem. Geol. 290, 31–49.
MacLean, W.H., 1990. Mass change calculations in altered rock series. Mineral. Deposita 25, 44–49.
Maynard, J.B., 1992. Chemistry of modern soils as a guide to interpreting Precambrian paleosols. J. Geol. 100, 279–289.
McLennan, S.M., 1989. Rare earth elements in sedimentary rocks; influence of provenance and sedimentary processes. Rev. Mineral. Geochem. 21, 169–200.
McLennan, S.M., 1993. Weathering and global denudation. J. Geol. 101, 295–303.
Mee, A.C., Bestland, E.A., Spooner, N.A., 2004. Age and origin of Terra Rossa soils in the Coonawarra area of South Australia. Geomorphology 58, 1–25.
Muhs, D.R., Budahn, J.R., 2009. Geochemical evidence for African dust and volcanic ash inputs to terra rossa soils on carbonate reef terraces, northern Jamaica, West Indies. Quat. Int. 196, 13–35.
Muhs, D.R., Budahn, J.R., Prospero, J.M., Carey, S.N., 2007. Geochemical evidence for African dust inputs to soils of western Atlantic islands: Barbados, the Bahamas, and Florida. J. Geophys. Res. 112.
Muhs, D.R., Budahn, J.R., McGeehin, J.P., Bettis, E.A., Skipp, G., Paces, J.B., Wheeler, E.A., 2013. Loess origin, transport, and deposition over the past 10,000 years, Wrangell-St. Elias National Park, Alaska. Aeolian Res. 11, 85–99.
Nesbitt, H.W., Young, G.M., 1984. Prediction of some weathering trends of plutonic and volcanic rocks based on thermodynamic and kinetic considerations. Geochim. Cosmochim. Acta 48, 1523–1534.
Nesbitt, H.W., Young, G.M., 1989. Formation and diagenesis of weathering profiles. J. Geol. 97, 129–147.
Olivarez, A.M., Owen, R.M., Rea, D.K., 1991. Geochemistry of eolian dust in Pacific pelagic sediments: implications for paleoclimatic interpretations. Geochim. Cosmochim. Acta 55, 2147–2158.
Panahi, A., Young, G.M., Rainbird, R.H., 2000. Behavior of major and trace elements (including REE) during Paleoproterozoic pedogenesis and diagenetic alteration of an Archean granite near Ville Marie, Québec, Canada. Geochim. Cosmochim. Acta 64, 2199–2220.
Porto, P., Wlling, D.E., Ferro, V., 2001. Validating the use of caesium-137 measurements to estimate soil erosion rates in a small drainage basin in Calabria, Southern Italy. J. Hydrol. 248, 93–108.
Quijano, L., Beguería, S., Gaspar, L., Navas, A., 2016. Estimating erosion rates using ^{137}Cs measurements and WATEM/SEDEM in a Mediterranean cultivated field. Catena 138, 38–51.
Rahimi, M.R., Ayoubi, S., Abdi, M.R., 2013. Magnetic susceptibility and Cs-137 inventory variability as influenced by land use change and slope positions in a hilly, semiarid region of west-central Iran. J. Appl. Geophys. 89, 68–75.
Riebe, C.S., Kirchner, J.W., Finkel, R.C., 2004. Erosional and climatic effects on long-term chemical weathering rates in granitic landscapes spanning diverse climate regimes. Earth Planet. Sci. Lett. 224, 547–562.
Song, C.S., Ji, H.B., Beckford, H.O., Chu, H.S., Zhang, K., Wang, S.J., 2018. Features of soil redistribution and major element migration in a karst hillslope of Southwest China. J. Mt. Sci. 15, 1892–1908.
Su, N., Yang, S.Y., Guo, Y.L., Yue, W., Wang, X.D., Yin, P., Huang, X.T., 2017. Revisit of rare earth element fractionation during chemical weathering and river sediment transport. Geochem. Geophys. Geosyst. 18, 935–955.
Taylor, A.S., Lasaga, A.C., 1999. The role of basalt weathering in the Sr isotope budget of the oceans. Chem. Geol. 161, 199–214.
Taylor, A.B., Velbel, M.A., 1991. Geochemical mass balances and weathering rates in forested watersheds of the southern Blue Ridge II. Effects of botanical uptake terms. Geoderma 51, 29–50.
Vance, D., Teagle, D.A., Foster, G.L., 2009. Variable Quaternary chemical weathering fluxes and imbalances in marine geochemical budgets. Nature 458, 493–496.
Walling, D.E., Quine, T.A., 1990. Calibration of caesium-137 measurements to provide quantitative erosion rate data. Land Degrad. Dev. 2, 161–175.
Walling, D.E., Quine, T.A., 1993. Use of Caesium-137 as a Tracer of Erosion and Sedimentation: Handbook for the Application of the Caesium-137 Technique. UK Overseas Development Administration Research Scheme R.
Wei, X., Ji, H.B., Li, D.J., Zhang, F.L., Wang, S.J., 2013. Material source analysis and element geochemical research about two types of representative bauxite deposits and terra rossa in western Guangxi, southern China. J. Geochem. Explor. 133, 68–87.
Xiong, K., Yin, C., Ji, H.B., 2018. Soil erosion and chemical weathering in a region with typical karst topography. Environ. Earth Sci. 77.
Yang, Q.Y., Xie, Y.Q., Li, W.J., Jiang, Z.C., Li, H., Qin, X.M., 2013. Assessing soil erosion risk in karst area using fuzzy modeling and method of the analytical hierarchy process. Environ. Earth Sci. 71, 287–292.
Yoo, K., Mudd, S.M., Sanderman, J., Amundson, R., Blum, A., 2009. Spatial patterns and controls of soil chemical weathering rates along a transient hillslope. Earth Planet. Sci. Lett. 288, 184–193.
Young, G.M., Nesbitt, H.W., 1998. Processes controlling the distribution of Ti and Al in weathering profiles, siliciclastic sediments and sedimentary rocks. J. Sediment. Res. 68, 448–455.
Zapata, F., 2002. Handbook for the Assessment of Soil Erosion and Sedimentation Using Environmental Radionuclides. Kluwer Academic Publishers, London, Vienna.
Zhang, X.B., Higgitt, D.I., Walling, D.E., 1990. A preliminary assessment of the potential for using caesium-137 to estimate rates of soil erosion in the Loess Plateau of China. Hydrol. Sci. J. 35, 243–252.
Zhang, X.B., Long, Y., He, X.B., Fu, J.X., Zhang, Y.Q., 2008. A simplified ^{137}Cs transport model for estimating erosion rates in undisturbed soil. J. Environ. Radioact. 99, 1242–1246.